Gastrointestinal involvement attenuates COVID-19 severity and mortality

Authors: Alexandra E. Livanos[1,2*], Divya Jha[1,2*], Francesca Cossarini[1,3*], Ana S. Gonzalez-Reiche[4*] Minami Tokuyama[1,2*], Teresa Aydillo[5,15*], Tommaso L. Parigi[6*], Irene Ramos[7], Katie Dunleavy[8], Brian Lee[9], Rebekah Dixon[2], Steven T. Chen[1,10], Gustavo Martinez-Delgado[1,2], Satish Nagula[2], Huaibin M. Ko[2,11], Jason Reidy[11], Steven Naymagon[2], Ari Grinspan[2], Jawad Ahmad[2], Michael Tankelevich[1,2], Ronald Gordon[11], Keshav Sharma[1,2], Graham J. Britton[1,12], Alice Chen-Liaw[1,12], Matthew P. Spindler[1,12], Tamar Plitt[1,12], Pei Wang[4], Andrea Cerutti[1,13,14], Jeremiah J. Faith[1,12], Jean-Frederic Colombel[1,2], Ephraim Kenigsberg[1,4], Carmen Argmann[4], Miriam Merad[1,8,9,10], Sacha Gnjatic[1,8,9,10,11], Noam Harpaz[11], Silvio Danese[6], Adeeb Rahman[1,4,9,10], Nikhil A. Kumta[2], Alessio Aghemo[6], Francesca Petralia[4†], Harm van Bakel[4,12†], Adolfo Garcia-Sastre[3,5,15†] and Saurabh Mehandru[1,2†]

* These authors contributed equally to this work.
† These authors contributed equally to this work.

Please address correspondence to:
saurabh.mehandru@mssm.edu,
adolfo.Garcia-Sastre@mssm.edu,
harm.vanbakel@mssm.edu, or
francesca.Petralia@mssm.edu

Authors affiliations

[1]Precision Immunology Institute, Icahn School of Medicine at Mount Sinai, New York, NY 10029
[2]The Dr. Henry D. Janowitz Division of Gastroenterology, Department of Medicine, Icahn School of Medicine at Mount Sinai, New York, NY 10029
[3]Division of Infectious Disease, Department of Medicine, Icahn School of Medicine at Mount Sinai, New York, NY 10029
[4]Department of Genetics and Genomic Sciences, Icahn School of Medicine at Mount Sinai, New York, NY 10029, USA.
[5]Department of Microbiology, Icahn School of Medicine at Mount Sinai, New York, NY 10029
[6]Department of Biomedical Sciences, Humanitas University, Milan, Italy.
[7]Department of Neurology and Center for Advanced Research on Diagnostic Assays, Icahn School of Medicine at Mount Sinai, New York, New York, 10029.
[8]Department of Medicine, Icahn School of Medicine at Mount Sinai, New York, NY 10029
[9]Human Immune Monitoring Center (HIMC) Icahn School of Medicine at Mount Sinai New York, New York, 10029
[10]Department of Oncological Sciences, Icahn School of Medicine at Mount Sinai, New York, NY, USA
[11]Department of Pathology, Icahn School of Medicine at Mount Sinai, New York, NY 10029
[12]Icahn Institute for Data Science and Genomic Technology, Icahn School of Medicine at Mount Sinai, New York, NY, 10029
[13]Catalan Institute for Research and Advanced Studies (ICREA), Barcelona, Spain
[14]Program for Inflammatory and Cardiovascular Disorders, Institut Hospital del Mar d'Investigacions Mèdiques (IMIM), Barcelona, Spain
[15]Global Health and Emerging Pathogens Institute, Icahn School of Medicine at Mount Sinai, New York, NY, USA.

A.E.L.: Gastroenterology Fellow, D.J.: Postdoctoral Fellow, F.C.: Assistant Professor, A.S.G-R.: Postdoctoral Fellow, M.T.: MD candidate, T.A.: Instructor, T.L.P.: Gastroenterology Fellow, I.R.: Assistant Professor, K.D.: Internal Medicine Resident, B.L.: Computational Scientist , R.D.: Senior Research Coordinator, S.T.C.: MD/PhD candidate, G.M.D.: Research manager, S.N.: Associate Professor, H.M.K.: Assistant Professor, J.R.: Electron Microscopist, S.N.: Assistant Professor, A.G.: Assistant Professor, J.A.: Professor, M.T.: Research Coordinator, R.G.: Research Professor, K.S.: Master's candidate, G.J.B.: Instructor, A.C.L.: MD/PhD candidate, M.P.S.: MD/PhD candidate, T.P.: PhD candidate, P.W.: Professor, A.C.: Professor, J.J.F.: Associate Professor, J.F.C.: Professor, E.K.: Assistant Professor, C.A.: Associate Professor, M.M.: Professor, S.G.: Associate Professor, N.H.: Professor, S.D.: Professor, A.R.: Associate Professor, N.A.K.: Associate Professor, A.A.: Associate Professor, F.P.: Assistant Professor, H.V.B.: Assistant Professor, A.G.S.: Professor, S.M.: Associate Professor.

Abstract

Given that gastrointestinal (GI) symptoms are a prominent extrapulmonary manifestation of coronavirus disease 2019 (COVID-19), we investigated the impact of GI infection on disease pathogenesis in three large cohorts of patients in the United States and Europe. Unexpectedly, we observed that GI involvement was associated with a significant reduction in disease severity and mortality, with an accompanying reduction in key inflammatory proteins including IL-6, CXCL8, IL-17A and CCL28 in circulation. In a fourth cohort of COVID-19 patients in which GI biopsies were obtained, we identified severe acute respiratory syndrome coronavirus-2 (SARS-CoV-2) within small intestinal enterocytes for the first time *in vivo* but failed to obtain culturable virus. High dimensional analyses of GI tissues confirmed low levels of cellular inflammation in the GI lamina propria and an active downregulation of key inflammatory genes including *IFNG*, *CXCL8*, *CXCL2* and *IL1B* among others. These data draw attention to organ-level heterogeneity in disease pathogenesis and highlight the role of the GI tract in attenuating SARS-CoV-2-associated inflammation with related mortality benefit.

Introduction

Coronavirus disease 2019 (COVID-19), is a multisystem illness caused by severe acute respiratory syndrome coronavirus 2 (SARS-CoV-2) a recently discovered novel betacoronavirus[1-3]. Manifestations of COVID-19 range from asymptomatic infection to severe, life-threatening disease with end-organ damage[3-5]. Common symptoms of COVID-19 include fever, cough, and shortness of breath that occur within 2 to 14 days after exposure to SARS-CoV-2[6]. A subset of COVID-19 patients also report gastrointestinal (GI) symptoms, comprising nausea, vomiting, diarrhea, abdominal pain and/or loss of appetite[7-11], which is not surprising given that the host receptor for SARS-CoV-2 (ACE2 receptor) is highly expressed on intestinal epithelium[12,13]. Several studies have demonstrated the presence of SARS-CoV-2 RNA in the fecal samples of infected persons[11,14-17] and in some cases even after clearance from respiratory samples[17]. Additionally, several members of the *Coronaviridae* family are known to be enterotropic, causing gastroenteritis in addition to respiratory illness[18]. Notably, SARS-CoV and MERS-CoV, closely related to SARS-CoV-2, have been identified in fecal samples of infected individuals[19-22]. Finally, the presence of GI involvement by SARS-CoV-2 has also been suggested by epidemiological[23], clinical[24], non-human primate[25] and *in vitro*[26-29] data. However, to date there is no evidence of SARS-CoV-2 infection of human enterocytes *in vivo* and there are no studies on the responses of the GI immune system, arguably the largest in the body, in COVID-19 patients.

Immune dysregulation has been suggested as a primary driver of morbidity and mortality in COVID-19. Several cytokines and other immunological parameters have been correlated with COVID-19 severity. Most notably, elevated IL-6, IL-8, IL-10, MCP-1 and IP-10 levels were detected in hospitalized patients, especially critically ill patients, in several studies, and are associated with ICU admission, respiratory failure, and poor prognosis[3,30-36]. Alongside this pro-inflammatory cytokine environment, significant immune cell alterations have been described such as lymphopenia, T and B cell activation and exhaustion[37], as well as altered frequencies of myeloid cells, including conventional dendritic cells (cDCs) and plasmacytoid dendritic cells (pDCs)[5,38,39].

Given the emerging evidence of enteric involvement by SARS-CoV-2, immune dysregulation in COVID-19 and the propensity of the GI immune system to suppress inflammation, we aimed to define the role of the GI tract in the pathogenesis of COVID-19. Here, we present findings on four well-characterized cohorts of COVID-19 patients hospitalized in tertiary care centers in New York City, USA and Milan, Italy, where we conducted high dimensional analyses of mucosal and systemic immune parameters and investigated disease outcomes associated with GI involvement in COVID-19 patients.

Results

Clinical characteristics of discovery cohort

We initiated a large, multi-cohort study to determine the role of the GI tract in the pathogenesis of SARS-CoV-2 infection. Our initial, 'discovery cohort' comprised 925 patients who tested PCR positive for SARS-COV-2 at the Mount Sinai Hospital (MSH) in New York City between April 1, 2020 and April 15, 2020. Among these 925 patients, 634 cases met our inclusion criteria of hospital admission, age > 18 years and having a multiplexed cytokine panel performed during their admission (**Supplementary Fig. 1**). The basic demographics and clinical characteristics are summarized in **Table 1**. Patients were 64 ± 16 years old (range 23-99 years) with 369 (58%) of the patients being male. The cohort comprised 28% Hispanic, 25% African American, 22% White and the remainder Asian or other based on patient's self-reported ethnicity. Comorbid illnesses included obesity (37%), hypertension (HTN) (36%) and diabetes mellitus (DM) (22%), similar to prior reports[40]. Fifty-four (9%) patients had mild disease, 361 (57%) moderate, 158 (25%) severe and 61 (10%) had severe COVID-19 with end organ damage (EOD) (**Table 2**, disease severity defined in Methods and **Supplementary Table 1**). During hospitalization, 110 patients were admitted to the ICU (17%) and 151 patients (24%) died by the end of data collection (6/15/2020) (**Table 2**).

We analyzed diarrhea, nausea and vomiting at the time of hospital admission. Two hundred and ninety-nine patients (47%) reported any GI symptoms (nausea, vomiting and/or diarrhea) with diarrhea being the most common (245 patients, 39%), followed by nausea (157 patients, 25%), and then vomiting (82 patients, 13%) (**Table 3**). Patients with GI symptoms were significantly younger (average age 61 years) than those without GI symptoms (average age 67 years) ($p<0.0001$) (**Table 1**). The distribution of race, ethnicity and co-morbid illnesses including obesity, HTN, DM and inflammatory bowel diseases (IBD) were comparable between those with GI symptoms and those without GI symptoms (**Table 1**).

COVID-19 severity was significantly reduced in patients with GI symptoms when compared to those without GI symptoms

In an effort to determine the association between GI symptoms and COVID-19 severity, we initially performed univariate analysis comparing the distribution of COVID-19 severities in patients with and without GI symptoms. Patients presenting with GI symptoms had less severe disease than patients without GI symptoms ($p<0.001$ Chi-square test). Importantly, mortality was significantly lower in COVID-19 patients with GI symptoms (15.7%) than those without GI symptoms (31.0%; $p<0.0001$ Fisher's exact test) (**Table 2, Fig. 1a**). Furthermore, each individual GI symptom

(nausea, vomiting and diarrhea) was associated with less severe disease ($p<0.02$ Fisher's exact test) and lower mortality ($p<0.001$ Fisher's exact test) (**Fig. 1a**). These findings were further emphasized by Kaplan-Meier estimates of survival over short-term follow-up of 25 days ($p<0.001$ log-rank test) (**Fig. 1b, Supplementary Fig. 2a**). Consistent with prior reports[35,40,41] older age and higher disease severity were associated with higher mortality in the discovery cohort (**Table 4**), providing validity to our findings.

Next, we decided to account for multiple comorbidities in determining the impact of GI symptoms on COVID-19 outcomes. Herein, we adjusted for age, body mass index (BMI), gender, race, diabetes, HTN, chronic lung disease and heart disease in a multivariate model to determine the impact of any GI symptoms and each of the individual GI symptoms (nausea, vomiting or diarrhea) on disease outcomes. In the multivariable models, any GI symptoms, diarrhea, nausea, and vomiting, were inversely associated with disease severity and mortality, while age and BMI were positively associated with these outcomes. African-American race was inversely associated with disease severity but not mortality (**Fig. 1c, Supplementary Fig. 2b, Supplementary Table 2).** Patients who presented with GI symptoms had 50% reduced odds of having severe disease (odds ratio of 0.56) and death from COVID-19 (odds ratio 0.54), compared to the patients who presented without GI symptoms (**Fig. 1d, Supplementary Table 2**).

An external validation cohort further confirms decreased mortality in COVID-19 patients with GI symptoms

Next, we sought an external validation cohort, distinct from the MSH discovery cohort, and studied well-characterized patients (n=287) from Milan, Italy, to determine the impact of GI symptoms on COVID-19 associated outcomes. In this cohort, GI symptoms on admission were characterized as presence (n=80, 27.9%) or absence of diarrhea on admission (**Table 5**). Consistent with the discovery cohort, patients with diarrhea on admission were significantly younger (60.6 ± 13.9 vs 65.5 ± 13.3 for patients without diarrhea, $p = 0.0056$) and had significantly lower mortality (10.0% in patients with diarrhea vs 23.7% in patients without diarrhea, $p=0.008$). Additionally, patients with diarrhea had lower composite outcome of mortality or ICU admission compared to those without diarrhea (20% vs 40%, $p=0.0014$) (**Table 5**). Distinct from the discovery cohort, the proportion of male patients was lower in those patients with diarrhea (57.5%) compared to those without diarrhea on admission (72%) ($p=0.0238$) (**Table 5**). Next, the association between diarrhea and mortality was evaluated by multivariate logistic regression adjusting for age, gender, BMI, diabetes, chronic heart and lung disease and other confounders. Even after adjusting for these covariates, the presence of diarrhea on admission was found to be significantly inversely

associated with mortality with a median odds ratio of 0.33 over 1000 bootstrap iterations (**Fig. 1e**).

Presence of GI symptoms can be used to predict reduced disease severity and mortality in patients with COVID-19 in a second validation cohort

After observing significantly reduced mortality in COVID-19 patients with GI symptoms in our discovery and external validation cohort, we developed a predictive model based on the discovery cohort and applied it to a distinct internal validation cohort comprising of 242 well-characterized patients with COVID-19, admitted between April 16, 2020 and April 30, 2020 to MSH. The inclusion of 'any GI symptoms' to a model consisting of age and BMI at baseline, improved the ability to predict severity and mortality with a median area under the curve (AUC) of 0.59 (age + BMI) vs. 0.64 (age + BMI + any GI symptoms) for disease severity and 0.70 (age + BMI) vs. 0.73 (age + BMI + any GI symptoms) for mortality (**Fig. 1f, Supplementary Table 3**). In addition, the effect of GI symptoms, age and BMI on the AUC was evaluated by excluding each variable one at a time from the model and calculating the consequent reduction in AUC. The exclusion of GI symptoms resulted in a significant reduction in AUC with a median value of 0.054 for disease severity and 0.03 for mortality. Notably, the effect of GI symptoms on the AUC was more dramatic than that of age (AUC reduction of 0.054 versus 0.025) for disease severity (**Fig. 1f, Supplementary Table 3**).

COVID-19 patients with GI symptoms have reduced levels of circulating cytokines associated with inflammation and tissue damage.

To gain mechanistic insights into significantly reduced COVID-19 severity and mortality across these three large cohorts, we began by analyzing systemic biomarkers, comparing patients with and without GI symptoms admitted to MSH (discovery and internal validation cohorts). Initially, we examined, a set of 4 cytokines, IL-6, IL-8, TNF-α, and IL-1β, measured on admission in all the patients as part of routine clinical care. IL-6, and IL-8 levels, known to be associated with poor survival[35] were found to be significantly reduced in circulation of patients with GI symptoms (FDR 10%) (**Supplementary Fig. 3, Supplementary Table 4).**

Next, to facilitate high dimensional analyses of potential immunological differences between patients with and without GI symptoms, we performed a validated, multiplexed proteomic assay (O-link), simultaneously quantifying 92 protein analytes in 238 patients (from among the discovery and internal validation cohorts; GI symptoms (n=104), no GI symptoms (n=134)) where serum samples were available for analyses. Unsupervised consensus clustering of these 92 analytes revealed six groups of analytes with similar expression patterns across all COVID-19

patients (**Fig. 2a, Supplementary Table 5**). Notably, analytes in clusters 5 and 6 displayed less correlation in patients with GI symptoms compared to those without GI symptoms (**Fig. 2a**, **Supplementary Fig. 4**). Next, we interrogated biological pathways over-represented in each cluster of soluble analytes. We found that the "KEGG Jak/Stat Signaling Pathway" was significantly enriched in Cluster 5; while the "Hallmark Inflammatory Response" pathway was significantly enriched in Cluster 4 (Fisher's exact test 10% FDR). These pathways were downregulated in patients displaying diarrhea symptoms based on pathway level signatures ($p<0.05$ from t-test) (**Fig. 2b**); suggesting a reduced inflammatory response in patients affected by GI symptoms. In addition, we found that clusters 1, 2, 3, 5 and 6 were significantly downregulated in patients with GI symptoms compared to those without (FDR 15%) (**Fig. 2c**). This downregulation seemed to be driven mostly by diarrhea since the same clusters 1, 2, 3, 5 and 6 were significantly downregulated with FDR correction at 10% in patients who presented with diarrhea compared to those without symptoms. The lack of signal registered for nausea and vomiting might be due to reduced statistical power given by the smaller number of samples displaying vomiting (n=29) or nausea (n=54) symptoms.

When looking at each of the 92 analytes individually, key inflammatory cytokines and chemokines were significantly downregulated (IL-8, TGF-α, IL-17C, IL-15RA, IL-10RB, MMP10, TNFRSF9, OPG, IL-6, LIF, GDNF, IL-17A, ARTN and CCL28). On the other hand, TNF-Related Apoptosis Inducing Ligand (TRAIL), a cytokine with immune regulatory properties[42,43] and IL-7, a cytokine associated with T cell development[44] were significantly upregulated in patients with GI symptoms compared to those without (t-test FDR 10%) (**Fig. 2d,e, Supplementary Table 6**). When looking at each individual GI symptom, diarrhea had the most significantly differential analytes. As a caveat, this difference between diarrhea, nausea and vomiting might be due to reduced statistical power given that fewer patients presented with nausea and vomiting than those who presented with diarrhea. Consistent with GI symptoms as a group, IL-7 was significantly increased, in addition, MCP-2 was significantly increased in patients presenting with diarrhea.

We also quantified total anti-spike protein IgA, IgG and IgM antibodies and compared patients with and without GI symptoms and patients with and without diarrhea. There were no significant differences between the groups (**Supplementary Fig. 5**)

Thus, overall, GI symptoms are associated with significantly reduced levels of key inflammatory cytokines like IL-6, IL-8, IL-17 and CCL28 that are known to be associated with poor COVID-19 outcomes.

The GI tract was endoscopically uninflamed in all patients

Next, we sought to obtain GI tissue-level mechanistic insights regarding disease pathogenesis. To this end, we enrolled 18 cases with COVID-19 and 10 SARS-CoV-2 uninfected controls who underwent upper GI endoscopy (SARS-CoV-2 infected n=16, uninfected n=8), colonoscopy (SARS-CoV-2 infected n=1, uninfected n=1) or both upper endoscopy and colonoscopy (SARS-CoV-2 infected n=1, uninfected n=1) (**Table 6, Supplementary Table 7**). Patient 10 was initially suspected to have COVID-19 but was excluded after multiple negative SARS-CoV-2 nasopharyngeal (NP) PCR tests and negative COVID-19 antibody tests. The remaining 17 cases were classified as asymptomatic / mild / moderate (n=10) or severe (n=7) disease according to the criteria detailed in **Supplementary Table 1**. While we endeavored to examine patients as early in disease course as was possible, given the aerosolizing nature of endoscopic procedures (potentially exposing endoscopic staff to SARS-CoV-2), as well as challenges inherent in endoscopic biopsies of acutely ill COVID-19 patients, a majority of patients were examined in the early convalescent phase of COVID-19 disease. Specifically, GI biopsies were performed after 27.5 $\pm$ 13.8 days from the onset of COVID-19 symptoms (or first SARS-CoV-2 PCR if asymptomatic) and 17.3 $\pm$ 17.5 days from the last positive NP swab (if patient had a positive NP swab after the procedure, it was considered to be 0 days from last PCR positive) (**Fig. 3a**). COVID-19 symptoms on presentation and treatment regimens were diverse as detailed in **Supplementary Table 8**. Sample allocation for different assays is detailed in **Supplementary Fig. 9**.

The GI mucosa was endoscopically uninflamed in all subjects regardless of the severity of illness, with no evidence of loss of vascularity, edema, friability, erosions or ulcerations (**Fig. 3b**), except for one post-intestinal transplant case where inflammation was attributed to transplant rejection. Histopathological examination revealed a mild increase in intraepithelial lymphocytes (IELs) in 8 cases and a scant neutrophilic infiltrate in 7 cases (**Fig. 3c**, **Supplementary Fig. 6**, **Supplementary Table 9**). Notably, the biopsies were reported as histologically normal in 3 cases (**Fig. 3d, Supplementary Table 9**). Histopathological details of pre-pandemic (non-COVID-19) controls are provided in **Supplementary Table 10**.

Small bowel enterocytes have robust expression of Angiotensin converting enzyme-2 (ACE2) and harbor SARS-CoV-2 antigens

Early events in the pathogenesis of SARS-CoV-2 infection include attachment of the receptor binding domain of the viral spike (S) protein to epithelial ACE2[14-17]. Using immunofluorescence (IF) microscopy, we observed robust and extensive expression of ACE2 on the small intestinal brush border in both COVID-19 cases and controls (**Fig. 4a-h**). Additionally, we detected SARS-

CoV-2 nucleocapsid protein in small intestinal enterocytes of COVID-19 patients (**Fig. 4i,n, Supplementary Fig. 7**), but not controls (**Fig. 4m,r, Supplementary Fig. 8**), indicative of virus infection in these cells. Remarkably, when present, the distribution of viral antigens was patchy in the upper small intestines (duodenum; **Fig. 4i-l**), but diffuse in the lower small intestines (ileum; **Fig. 4n-q**). Positive staining was exclusively seen in the epithelium irrespective of intestinal location. Overall, of the 11 COVID-19 patients where IF staining was performed, 10 showed viral antigen on IF microscopy in at least one intestinal segment (duodenum or ileum) (**Supplementary Table 9**). Interestingly, the presence of viral antigens on IF did not correlate with the presence of histologic abnormalities. As negative controls, 5 duodenal biopsies and 6 ileal biopsies from 10 patients collected prior to the pandemic (**Supplementary Table 10**), showed no evidence of viral antigens on immunostaining (**Fig. 4m,r, Supplementary Fig. 8**).

Ultrastructural analyses of GI tissues reveal viral particles in small intestinal enterocytes

Transmission electron microscopy of intestinal biopsy tissues revealed the presence of 70-110 nm viral particles in the enterocytes of the duodenum and ileum (**Fig. 4s-u**). Pleomorphic, spherical structures, morphologically consistent with viral particles were observed in conjunction with small vesicles within enterocytes along the basolateral surface of the enterocytes (**Fig. 4s**) and blebbing off of the enterocyte apex (**Fig. 4u**). Particles with distinct, stalk-like projections (corona) were seen within the enterocyte cytoplasm (**Fig. 4t**). Overall, of the 13 patient samples processed for electron microscopy studies, 6 showed viral-like particles on ultrastructural analyses (**Supplementary Table 9**).

Infectious virions could not be isolated from the GI tissues of COVID-19 patients

Several attempts were made to assess for the presence of potentially infectious virions in the intestines of COVID-19 patients. Supernatants of homogenized intestinal tissues were inoculated on confluent Vero E6 cells and incubated at 37℃ for 7 days. Brightfield microscopy showed no apparent cytopathic effects (CPE). In addition, cell culture supernatants did not reveal the presence of viral RNA by quantitative RT-PCR (qRT-PCR) and plaque assays. Experiments showed no plaque formation in Vero E6 cells after staining with 2% crystal violet solution.

RT-qPCR was performed in whole biopsy tissue after RNA isolation in both COVID-19+ patients and controls. Results showed that Ct values of COVID-19+ patients were ≥34, while RNA sequencing (RNA-Seq) data detected SARS-CoV-2 reads only in the one ileal sample tested but in none of the 12 duodenal biopsies. Altogether these data suggest that SARS-CoV-2 was present at low copy numbers in the GI tract of these early-convalescent COVID-19 cases.

GI lamina propria pro-inflammatory dendritic cells are depleted in COVID-19 patients

Next, we performed mass cytometry (CyTOF) based immunophenotypic analyses on the GI tissues of 13 and peripheral blood of 10 COVID-19 cases and 10 controls (**Table 6, Supplementary Table 7, Supplementary Fig. 9**). GI tissues were divided into lamina propria (LP) and epithelial compartment (EC) fractions and analyzed separately. Immune populations were clustered on the basis of cell-specific markers for both the LP and EC (**Fig. 5a,c,g**). While the overall distribution of canonical immune cell subsets in the GI LP were comparable between COVID-19 and control patients (**Fig. 5a,b**), few immune populations showed differences as detailed below. Additionally, no clear differences in the LP could be discerned between patients with asymptomatic/mild/moderate disease and those with severe disease (**Fig. 5b, Supplementary Table 12a**).

In the LP, among myeloid cells, $CD206^+CD1c^+$ "inflammatory" cDC2 (conventional DCs)[45] were reduced in COVID-19 cases compared to controls (0.4-fold decrease, p=0.01). Additionally, plasmacytoid DCs (pDCs) were reduced in COVID-19 cases (0.5 fold decrease, p=0.07) (**Fig. 5d,e**), analogous to changes described in the peripheral blood of COVID-19 patients[36]. Among other LP populations, effector ($PD\text{-}1^+CD38^+$) $CD4^+$ and $CD8^+$ T cells were significantly increased in COVID-19 cases compared to the controls (**Fig. 5f**), while $CD8^+CD103^+$ T cells (tissue resident memory subset) trended higher in COVID-19 cases compared to controls (1.7-fold increase, p=0.06) (**Supplementary Fig. 10a**). Neutrophils (3-fold), eosinophils (1.9-fold), $CD4^-CD8^-$T cells (3.5-fold) and $CD4^+CD103^+$ T cells (1.8-fold) were increased in COVID-19 cases, but these differences were not statistically significant possibly due to the sample size. We also observed a trend of non-significantly decreased regulatory $CD4^+$ T (T_{REG}) cells (0.6-fold decrease) and increased IgM^+ plasma cells (2.3-fold increase) in the LP of infected cases vs controls (**Supplementary Fig. 10a**). The distribution of naïve and memory $CD4^+$ and $CD8^+$ T cells was altered in COVID-19 patients, with a reduction of naïve $CD4^+$ T cells and EMRA (effector memory re-expressing RA) $CD8^+$ T cells in LP of COVID-19 patients (**Supplementary Fig. 10b**), but this difference did not reach statistical significance.

Similar to the LP, the EC showed a reduction of $CD206^+$ cDC2 in COVID-19 cases compared to controls (0.4-fold decrease, p=0.05), while the $CD4^-CD8^-$ subset of IELs was significantly increased (1.6-fold-increase, p=0.03) (**Fig. 5h**). $CD8^+$ T cells, the dominant IEL population, showed an increase (2.6-fold) in COVID-19 cases compared to controls but the difference did not reach statistical significance (p=0.4) (**Supplementary Table 12a**), likely owing to inter-patient variability, also observed by light microscopy. A subset of $CD8^+$ IELs, $CD8^+CD69^+$

T cells, showed a non-significant increase in COVID-19 cases vs controls (3.9-fold, p=0.2), while plasma cells were comparable between the cases and controls (**Supplementary Fig. 11 a,b,c)**.

In the peripheral blood, cell type assignments were carried out using specific cell surface markers (**Supplementary Fig. 12a**). We observed that effector (PD-1^{+}CD38^{+}) T cells (for both CD4^{+} and CD8^{+} T lymphocytes) were significantly increased in PBMCs of SARS-CoV-2 infected individuals (**Fig. 5i**). CD14^{-}CD16^{+} inflammatory monocytes trended lower in COVID-19 cases compared to controls (0.4-fold decrease, p=0.09). In contrast, CD14^{+}CD16^{-} "classical" monocytes were comparable in COVID-19 cases and controls (p=0.3) (**Supplementary Fig. 12b**). Additionally, a non-significant increase in IgG^{+} plasma cells (7.2-fold, p=0.13) and a non-significant decrease in T_{REG} (0.8-fold, p=0.2) were observed in COVID-19 cases (**Supplementary Fig. 12c,d, Supplementary Table 12b**). Finally, a significant increase in activated (CD29^{+}CD38^{+}) CD4+ T cells was noted in the peripheral blood of COVID-19 cases compared to controls (**Supplementary Fig. 13a)** and a non-significant increase of these activated T cells in the LP of COVID-19 patients (**Supplementary Fig. 13b**)**.** Details of all immune population changes in the GI LP, GI EC and in circulation are provided in **Supplementary Table 12a and 12b**.

Altogether, similar to published data from the peripheral blood of COVID-19 patients[36], intestinal tissues from COVID-19 cases showed reduced pro-inflammatory DCs and pDCs but increased effector T cells compared to controls.

GI LP pro-inflammatory pathways are downregulated in COVID-19 patients

To further probe the molecular response of the GI tract following SARS-CoV-2 infection, we performed RNA-Seq on EC and LP cellular fractions separately in 13 COVID-19 patients and 8 controls. Samples derived from the EC and LP clustered separately on the basis of their top transcriptional signatures, demonstrating distinctness of the two compartments within the GI tract (**Supplementary Fig. 14, Supplementary Data**). Accordingly, comparisons between COVID-19 cases and controls were performed separately for each tissue, and 1063 differentially expressed genes (DEG) were identified out of total 11419 genes detected (**Fig. 6a, Supplementary Data**). The majority of DEGs were detected in the LP (1061, false discovery rate [FDR] ≤ 0.05), compared to 12 DEGs in the EC that largely overlapped with the LP (**Fig. 6a**). Both LP and EC showed upregulation of genes involved in immunomodulation, including the anti-microbial peptide *LCN2*, and the metallothioneins *MT1E*, *MT1F*, *MT1H*, *MT1M*, *MT1X*, *MT2A* and *TMEM107.* In addition, heat shock proteins, *HSPA1A* and *HASPA1B,* were downregulated in both tissues. Pathway enrichment analysis of DEGs ranked by significance revealed several KEGG pathways that were depleted in COVID-19 patients compared to controls (**Fig. 6b)**. Downregulation of pathways linked

to T_H17 cell differentiation and inflammatory bowel diseases (IBD) was characterized by the depletion of *RORA, IL4R, IFNG, IL18R1, IL1B, STAT4* and *HLA-DRA*. Pathways linked to antigen processing, T_H1 and T_H2 cell differentiation, and MAPK signaling were significantly downregulated in the LP from COVID-19 patients. In contrast, genes associated with metabolic functions, including amino acid metabolism (*NOS2, SMS, ALDH2, GOT2*), mineral absorption (*MT1G, MT2A, MT1E*), as well as mucin biosynthesis (*GALNT7, GALNT3, GALNT8*) were significantly upregulated in COVID-19 patients compared to controls (**Fig. 6b**).

We considered the possibility that the observed expression changes could imply alterations in relative cell type proportions (in addition to transcriptional alterations within cells). Therefore, we interrogated GI data derived from single-cell RNA-seq[46] for enrichment of cell type-specific gene expression signatures. Consistent with CyTOF data (**Fig. 5** and **Supplementary Table 12a and 12b**), genes associated with DCs and eosinophils were reduced in COVID-19 patients compared to controls (**Fig. 6c**). Additionally, signatures related to the size of endothelial cell and mast cell pools were reduced, while genes linked to goblet cells, proliferating epithelial cells, enteroendocrine cells and epithelial stem cells were increased, possibly reflecting the sequelae of intestinal epithelial infection by SARS-CoV-2 and subsequent recovery (**Fig. 6c**).

Given the unexpected reduction in DC numbers in the GI tissues, we probed myeloid gene signatures further, and found significant downregulation of genes associated with pDC *(DAPK1, IRF7, ICAM1* and *GM2A*), activated DCs (*TNFAIP2, CD86, CD83*), cDC1 (*RELB, IRF8* and *HLA-DRA*) and cDC2 (*CLEC7A* and *CLEC10A*). Of note, we also found that LP genes associated with inflammatory DCs (monocyte-derived DCs, MoDCs) (*TGFBI, TGFB1, STAB1, SDCBP, RNASET2, MSR1, MRC1, MERTK, DNASE1L3, CD163L1, C5AR1, SPI1, CSF1R, AOAH, ABCA*) were significantly reduced (**Fig. 6d**), which was consistent with the reduced number of inflammatory DCs observed by CyTOF.

Finally, we looked at the average EC and LP expression of recently reported gene signatures linked to the antiviral response against SARS-CoV-2 from post-mortem lung tissue samples[30], and human intestinal organoids[29]. Although we did not observe a substantial acute SARS-CoV-2 response, there was significant upregulation of *LCN2* in both EC and LP, and *OAS* and *GBP3* in the LP only. Notably, we did observe a trend towards induction of antiviral response genes in the EC, where expression of canonical antiviral genes such as *IFI44L, IFIT1, IFITM3, IFI44, IFI6* and *OAS3* was increased (**Fig. 6e**).

Next, using gene set enrichment analysis (GSEA), we rank ordered the EC DEGs according to effect size (logFC * -logPvalue) and tested for enrichment in the reported SARS-CoV-2 infected gene signatures[29] (**Supplementary Fig. 15a**). The genes upregulated in EC

showed a significant enrichment in genes upregulated in the SARS-CoV-2 infected intestinal organoid gene datasets. We then carried out Hallmark pathway enrichment analyses on this ranked EC gene list and found that the top two processes associated with genes upregulated in EC were interferon alpha response (normalized enrichment score (NES) 1.91, FDR<0.005) and interferon gamma response (NES=1.8, FDR=0.005) (**Supplementary Fig. 15b**). This enrichment is indicative of the host antiviral response against SARS-CoV-2 in human intestines of COVID-19 patients.

We then evaluated cytokines and chemokines in intestinal samples projecting our RNA-seq dataset with published data from the human bronchial epithelial cells infected with SARS-CoV-2[30]. Remarkably, we found that the many of the inflammatory cytokines and chemokines such as IL-1β, IFNγ, CCL24 and CXCL8 were downregulated in COVID-19 patients (**Fig. 6e**). The only chemokine showing significant increase was CCL15 which is reported to have structural properties of antimicrobial peptides and has a role in maintaining intestinal homeostasis[47] (**Fig. 6e**). Significantly, we also noted that the key inflammatory genes including *IFNG, IL1B, CXCR4, TNFSF14, CXCL2, CSF-1, CXCL8, IL18R1, NRP1 and IL18BP* were downregulated in intestinal LP of COVID-19 cases compared to the uninfected controls (**Fig. 6f**).

Together, these data reveal a dynamic remodeling of GI tissues by SARS-CoV-2, notable in the LP for a significant downregulation of pathways associated with inflammation and antigen presentation, yet activation of viral response signaling genes in the EC.

Discussion

At the outset, given the robust expression of ACE2 on the small intestinal epithelium[48], at levels that are arguably among the highest in the body[49], we hypothesized that the GI tract would be susceptible to SARS-CoV-2 infection. In testing our hypothesis, herein, we report on the first human study to demonstrate infection of intestinal enterocytes *in vivo*, define the cellular and transcriptomic responses of GI tissue in COVID-19 patients and associate them with clinical outcomes in multiple, large cohorts of COVID-19 patients. An unexpected, but significant reduction in disease severity and mortality in patients with GI symptoms identifies a new aspect of disease pathogenesis and provides evidence of an 'organ-specific' program of host response to SARS-CoV-2, which in this case is associated with a survival advantage.

GI manifestations, reported in nearly half of patients within our discovery cohort were notably higher than some of the early reports[3,7] but similar to more recent studies[8], likely attributable to greater clinical awareness of GI symptoms and therefore more documentation of such symptoms. A recently published study of 278 patients from a Columbia University Hospital

in New York City reported that among COVID-19 patients with GI symptoms (diarrhea, nausea and vomiting), there was a non-significant trend towards lower rates of intensive care unit (ICU) admission and a significantly lower rate of death during short-term follow-up[50]. Similar observations arise from the study of 'Multisystem Inflammatory Syndrome Children' (MIS-C). Some of these children have diarrhea as a predominant symptom[51,52], systemic evidence of GI involvement[9,53,54], and a unique responsiveness to anti-inflammatory treatments, including IL-6, intravenous immunoglobulin (IVIG) and anti-IL1[55-58], which lead to the resolution of inflammatory pathology in these children. Intestinal involvement in COVID-19 resulting in mortality benefit stands in contrast to the involvement of all other organs including the pulmonary[59,60], renal[61,62] and vascular[63] compartments.

The fact that GI symptoms remain significantly associated with better COVID-19 outcomes after adjusting for multiple covariates, known to be associated with reduced survival, in 3 independent cohorts totaling 1163 patients, across two different countries enhances the robustness and validity of our findings. Furthermore, our model to predict COVID-19 severity and mortality was enhanced by the inclusion of GI symptoms suggesting that intestinal parameters should be considered in initial assessments and severity stratification of COVID-19 patients.

Several, non-mutually exclusive hypotheses may explain the lower mortality in COVID-19 patients with GI symptoms. Possibilities include "diversion" of the virus away from the lung, an organ where infection proves lethal in a subset of patients. Another possibility includes virus intrinsic factors, associated with differences in tissue-tropism and perhaps virulence. Yet another intriguing possibility is that GI infection stimulates an anti-inflammatory, 'tolerogenic' immune response locally as well as systemically. Detailed examination of soluble, cellular and transcriptomic factors associated with GI infection provided some support for this argument.

For example, independent of disease severity and unlike inflammatory changes seen in the pulmonary mucosa[64], inflammatory infiltrates were scarce in the LP of COVID-19 patients. A patchy and mild increase in IELs was observed within the EC. Additionally, we observed a rather significant lack of cDC2, 'inflammatory' DCs, pDCs in the intestinal LP. These findings mirror observations from the SARS epidemic of 2003[19] as well as current autopsy data demonstrating a lack of intestinal inflammation despite the presence of viral antigens in both these tissues[65]. We propose that, in spite of their infectability, the intestines mount a limited and short-lasting inflammatory response to SARS-CoV-2.

On examination of circulating proteins, including analyses of cytokines and chemokines known to be associated with COVID-19 severity[30,31,35], we found that multiple cytokines/chemokines were downregulated in patients with GI symptoms compared to patients

without. These included the proinflammatory cytokines IL-6 and IL-8, which are now considered a hallmark of increased severity and mortality in COVID-19 as well as a number of other cytokines/chemokines involved in tissue inflammation. The lower IL-17 expression we observed systemically is in line with the reduced T_H17 RNA seq expression signatures we found in biopsy samples from COVID-19 patients. IL-17 is secreted by T_H17 and innate cells and is crucial for the recruitment of neutrophils promoting inflammation in a variety of tissues, including the intestinal mucosa[66,67]. Additionally, IL-17 has been shown to have pathogenic effects both in SARS-CoV-2[68] as well as during SARS-CoV[69] and MERS[70] infections. Interesting, IL-17C (specifically found to be decreased in patients with GI symptoms in our study) is produced primarily by epithelial cells rather than hematopoietic cells[71]. Our finding of COVID-19 patients with GI symptoms having reduced CCL28, a cytokine expressed by mucosal epithelial cells and involved in eosinophil chemotaxis[72], is consistent with prior work showing increased eosinophils to be associated with severe COVID-19 disease[31] and our RNA-seq data showing decreased eosinophil associated genes. IL-15 promotes neutrophilic cytoplasmic re-arrangements and phagocytosis[73], DCs differentiation[74], and T cell stimulation[75]. The reduced systemic expression of the IL-15 receptor is in line with our intestinal findings showing lower frequencies of DCs in COVID-19 patients. IL-10 is generally considered an immune modulatory and anti-inflammatory cytokine, however an excess of IL-10 can inhibit the function of immune cells such as NK and CD8+ T cells, possibly delaying clearance of viruses[76]. Our results of increased systemic expression of IL-10 receptor in patients presenting without GI symptoms is in line with previous studies showing IL-10 to be elevated in COVID-19 patients, associated with disease severity and inversely correlated with $CD8^+$ T cells[77,78].

In contrast, the only two cytokines found to be upregulated in patients presenting with GI symptoms were IL-7 and TRAIL, both with important immunoregulatory functions. IL-7, produced by stromal cells and intestinal epithelial cells, has been considered as a therapeutic agent in COVID-19 related to its effects on T cell differentiation and survival[79]. Similarly, TRAIL is associated with immunosuppressive, immunoregulatory and anti-inflammatory functions[42,43] as well as some evidence of viral infection control in the intestinal tract[80].

Transcriptome analyses further demonstrated the downregulation of a number of important pro-inflammatory gene products, including *IFNG*, *IL1B*, *IKBKB* and *STAT3B, which* contribute to T_H17 cell differentiation and IBD pathogenesis. Calprotectin, a heterodimer encompassing calgranulin A and calgranulin B, which are encoded by *S100A8* and *S100A9*, respectively, was recently identified as a biomarker of severe COVID-19 disease and suggested to represent a trigger of cytokine release syndrome[81]. We observed no induction of *S100A8* or

562 *S100A9* in intestinal tissues, even in patients with severe COVID-19, suggesting that the vast
563 intestinal surface did not contribute to the production of calprotectin in COVID-19 patients. Pro-
564 inflammatory cytokines and chemokines that are elevated in the lungs of COVID-19 patients[64,82]
565 were surprisingly downregulated (*IL1B, CXCL8, CXCL2, CXCR6*) or unchanged (*CCL3*, *CXCL10,*
566 *CCR1, CXCR3*) in the intestines, compared to non-COVID controls. Other relevant gene products
567 associated with severe COVID-19[64,83,84] were either significantly lower in the intestinal LP
568 (*CXCL8*, *IL1B, IFNG, HIF1A, HLA-DQA1*) or trended lower (*CCL2*, *CCL4*, *CCL4L2*, *CTSB*, *IL23A*)
569 or were comparable to non-COVID controls (*HMGB1*, *CCL3*, *CCL8*, *HMOX1*). Tissue-residence
570 markers such as *ITGA1*, *CXCR6*, *JAML*, which are reported to be increased in the pulmonary
571 mucosa of severe COVID-19 patients[64], were significantly downregulated in the GI tract. Finally,
572 aside from detecting decreased expression of pro-inflammatory gene products, we found
573 increased expression of anti-inflammatory gene products, including transcripts involved in the
574 biogenesis of the gut-specific MUC2 mucin, a mucus-forming glycoprotein released by goblet
575 cells that contributes to gut tolerance[85].

576 Thus, by dissecting circulating proteomic and GI tissue transcriptomic response, we noted
577 a cytokine milieu characterized by either a suppression of or a failure of induction of an
578 inflammatory response to the virus. Additionally, we observed a lack of production of secondary
579 mediators including calprotectin, which would feed into the inflammatory cascade and culminate
580 in the “cytokine storm” typical of severe COVID-19. Our detailed cellular analyses confirm a lack
581 of inflammatory monocytes and macrophages and a depletion of inflammatory DCs in the GI tract.
582 This failure of induction of inflammatory pathways, regardless of the clinical severity of disease,
583 stands in stark contrast to the massive immunopathology, noted systemically, and within the
584 pulmonary mucosa of severe COVID-19 patients[60] as well as patients with active IBD[86,87].

585 The mechanisms underpinning the lack of inflammation in the COVID-19-infected intestine
586 are unclear, but could be linked to the notorious tolerogenic bias of both effector and regulatory
587 cells from both innate and adaptive branches of the mucosal immune system[88]. In addition, the
588 SARS-CoV-2 virus could specifically inhibit immune activating and/or stimulate immune
589 suppressive pathways in the intestinal mucosa directly or indirectly through ACE2 or other
590 receptors. We also recognize that our analyses of the GI tract were not performed during the most
591 acute phase of the illness in some patients. However, even in the patients that were sampled
592 within the first 15 days of the onset of symptoms or positive nasal swab (patients 1, 6 and 18),
593 the “pro-inflammatory changes” were not observed in the intestines. A separate study by our
594 group that analyzed stool samples from patients going through the acute phase of COVID-19,
595 found little evidence of an active gut inflammatory response. In particular, such stool samples

596 strikingly lacked any significant increase of IL-1β, IL-6, TNF-α and IL-10, despite the detection of
597 viral genomes (MEDRXIV/2020/183947).

598 In summary, we have observed an unexpected but significant reduction in COVID-19
599 severity and mortality when patients demonstrate GI symptoms like diarrhea, nausea or vomiting.
600 These data suggest a previously unappreciated tissue-specific response to SARS-CoV-2 and
601 provide the rationale for more studies aimed at determining the mechanisms underpinning the
602 attenuation of SARS-CoV-2 pathogenicity by the intestinal environment. Such efforts may lead to
603 the development of novel treatments against COVID-19 and potentially other similar deadly
604 infections in the future.

605

606 **Methods**

607 **Clinical cohorts**

608 *1. Discovery cohort*

609 Patients admitted to Mount Sinai Hospital (MSH) between April 1, 2020 and April 15, 2020 were
610 recruited into the Discovery Cohort if they were SARS-CoV-2 PCR positive, more than 18 years
611 of age and if the "ELLA panel of cytokines" (IL-6, IL-8, IL-1β and TNF-α) was performed as part
612 of clinical care. Clinical details from eligible patients were extracted from Mount Sinai Data
613 Warehouse (MSDW) under an IRB approved protocol (IRB-20-03297A North American registry
614 of the digestive manifestations of COVID-19)

615 A total of 634 subjects were included in the discovery cohort (**Supplementary Figure 1**).
616 In addition to demographic information (including race and ethnicity and primary language),
617 clinical characteristics, laboratory data and outcomes data was extracted from the medical charts.
618 Co-variates that were studied included: history of smoking, BMI (obesity defined as BMI >30) and
619 comorbid conditions including, hypertension, diabetes, chronic lung disease (including asthma
620 and COPD), heart disease (including coronary artery disease, atrial fibrillation and heart failure),
621 chronic kidney disease, cancer, HIV, and inflammatory bowel disease (IBD).

622 COVID severity was defined based on internal scoring system developed by the
623 Department of Infectious Diseases at Mount Sinai Hospital with the following definitions: Mild -
624 SpO2>94% on room air AND no pneumonia on imaging, Moderate - SpO2<94% on room air OR
625 pneumonia on imaging, Severe - high flow nasal cannula (HFNC), non-rebreather mask (NRBM),
626 Bilevel Positive Airway Pressure (non-invasive positive airway ventilation), or Mechanical
627 ventilation AND no pressor medications AND creatinine clearance > 30 AND ALT < 5x upper limit
628 of normal, Severe with evidence of end organ damage (EOD) - high flow nasal canula (HFNC),
629 non-rebreather mask (NRBM), Bilevel Positive Airway Pressure (non-invasive positive airway

ventilation), or Mechanical ventilation AND pressor medications OR creatinine clearance <30 OR new renal replacement therapy OR ALT > 5x upper limit of normal.

GI symptoms were defined as more than one episode of either diarrhea, nausea, and/or vomiting at the time of admission. If only one episode of either diarrhea, nausea, and/or vomiting was specifically documented, patients were not considered to have GI symptoms. Additionally, we did not consider GI symptoms that developed during the course of hospitalization, as they could reflect nosocomial or treatment-related effects.

Disease severity (as described above) and mortality were considered as outcomes variables. Mortality was calculated as patient status (dead or alive) at 25 days post admission. If no information was available after discharge, patients were censored at the time of hospital discharge.

2. External Validation Cohort

To confirm the Discovery Cohort findings, we analyzed a cohort of patients admitted to a tertiary care center in Milan, Italy between February 22, 2020 and March 30, 2020. A total of 287 patients with a confirmed positive SARS-CoV-2 PCR and who did not die or were not transferred to the ICU within 24 hours from admission were studied. Presence of vomiting and diarrhea (defined as at least three loose bowel movement per day) on or prior to admission was recorded. Outcomes were analyzed using ICU admission, death or the composite study end-point of ICU admission or death within 20 days of hospitalization.

3. Internal Validation Cohort

To test a predictive model of COVID-19 severity and disease-related mortality, we developed a distinct 'Internal Validation Cohort' of patients who were hospitalized at MSH between April 16, 2020 and April 30, 2020 and satisfied the same inclusion and exclusion criteria as in the discovery cohort. Additionally, patients already included in the discovery cohort were excluded. From a total of 408 patients, 242 met inclusion criteria and were thus included in the Internal Validation Cohort. Demographic, clinical and outcomes related data was extracted from patients' medical records as described for the Discovery Cohort.

4. Intestinal Biopsy Cohort

To gain mechanistic insights into GI tissue response in COVID-19 patients, intestinal biopsies and peripheral blood from 18 COVID-19 and 10 control patients were obtained between April 17, 2020 and June 2, 2020. Subjects included hospitalized patients as well as those seen in the outpatient GI practices. COVID-19 cases and controls were defined on the basis of SARS-CoV-2 swab tests. The demographic characteristics of these patients and controls are provided in **Fig. 3a, Table 6,**

and **Supplementary Table 7**. Informed consent was obtained from all patients. The biopsy-related studies were approved by the Mount Sinai Ethics Committee/IRB (IRB 16-0583, The impact of viral infections and their treatment on gastrointestinal immune cells).

SARS-CoV-2 testing

The SARS-CoV-2 PCR was run in the Clinical Microbiology laboratory as part of routine care on the Roche cobas platform. This platform performs selective amplification of 2 targets ORF-1 (Target 1) and the E-gene for pan-Sarbecovirus (Target 2) (detects SARS-CoV-2 as well as SARS or MERS viruses, but not routine seasonal Coronavirus). A positive result indicated that either both Target 1 and Target 2 were detected (majority of cases) or Target 1 alone was detected. A presumptive positive result indicates a negative Target 1 result and a positive Target 2 result which according to the manufacture can be a result of the following: “1) a sample at concentrations near or below the limit of detection of the test, 2) a mutation in the Target 1 target region in the oligo binding sites, or 3) infection with some other Sarbecovirus (e.g., SARS-CoV or some other Sarbecovirus previously unknown to infect humans), or 4) other factors." Patients with a presumptive positive SARS-CoV-2 PCR were included in the analysis if they were treated clinically as having COVID-19.

Computational analyses

Descriptive statistics

Basic demographics and clinical characteristics of the cohort were defined by descriptive statistics. For univariable analyses graph pad prism (version 8) was used to perform statistical analyses and to produce figures. For age, an unpaired t-test was performed. For categorical variables, the Fisher’s exact test or the Chi-square test was used as appropriate.

Multivariate model based on discovery cohort

For this analysis, we considered 570 patients with clinical descriptors including as age, gender, race, BMI, comorbidities and GI symptoms. A multivariate logistic regression was utilized to model severity and mortality as function of each of the GI symptoms and clinical variables including race, age, gender, BMI, heart and lung diseases and hypertension. In particular, race was stratified as White (Caucasian), Black (African-American), Hispanic and others; lung disease was set equal to 1 if the patient was either affected by COPD or asthma and zero otherwise; heart disease was set equal to 1 if the patient was either affected by coronary artery disease, atrial fibrillation or heart failure and 0 otherwise. The severity indicator was set equal to 1 for severe and severe with EOD patients and 0 for Mild and Moderate COVID patients; mortality was set equal to 1 for deceased

patients and 0 otherwise. Significant association based on 95% confidence interval (CI) are reported in **Fig. 1c** and **Supplementary Table. 2**. CI of odds ratio were computed based on 1000 bootstrap iterations. At each bootstrap iteration, patients were sampled with replacements and logistic regressions were estimated considering as outcome severity and mortality. Then, 95% CI of coefficients and odds ratio were estimated across bootstrap iterations (**Fig. 1d**).

External Validation Cohort

For this analysis, we considered 228 patients with clinical data such as age, gender and GI symptoms. A multivariate logistic regression was utilized to model mortality, ICU admission and the composite outcome of ICU admission or mortality as function of presence or absence of diarrhea and clinical variables including age, gender, BMI, heart disease, COPD, diabetes and hypertension. Heart disease was set equal to 1 if the patient was either affected by coronary artery disease or atrial fibrillation and 0 otherwise. Confidence intervals of odds ratio were computed based on 1000 bootstrap iterations. At each bootstrap iteration, patients were sampled with replacements and logistic regressions were estimated considering the outcome as mortality, ICU admission or the composite outcome of ICU admission or death. Then, 95% confidence intervals of odds ratio were estimated across bootstrap iterations (**Fig. 1e**).

Predictive performance based on the Internal Validation Cohort

For this analysis, we considered 233 patients with clinical data including age, BMI, and GI symptoms. In order to evaluate the predictive performance of each model, bootstrapping was performed. Specifically, at each bootstrap iteration, we randomly sampled patients in the discovery cohort with replacement and estimated a logistic regression to model each outcome as function of a particular GI symptom, age and BMI. In this analysis, only age and BMI were adjusted for since they were the only variables significantly associated with both outcomes across different GI symptoms models in the discovery cohort (**Fig. 1c).** Then, the estimated model was utilized to predict the outcome of patients in the validation cohort. This procedure was repeated for 1000 bootstrap iterations. For each iteration, Receiving Operating Characteristic (ROC) curve and area under the curve (AUC) were computed. For comparison purposes, the distribution of AUC across 1000 bootstrap iterations from the predictive model based on age and BMI only was considered. **Fig. 1f** (left panel) shows the boxplot of AUC values across 1000 bootstrap iterations. Then, considering the following model

$$\text{outcome} = f(\text{age} + \text{bmi} + \text{any GI symptom}) \qquad \text{[Model 1]}$$

we evaluated the effect of each variable on the outcome by computing the reduction in AUC obtained after removing one variable at a time. For this purpose, the AUC of model [Model 1] was compared to the following three models

outcome = f(age + bmi) [Model 2]

outcome = f(age + any GI symptom) [Model 3]

outcome = f(bmi + any GI symptom) [Model 4]

for 1000 bootstrap iterations. Following the strategy above, at each bootstrap iteration, patients were sampled with replacement. **Fig. 1f** (right panel) shows the 95% confidence intervals of difference in AUC between [Model 1] and [Model 2], [Model 3] and [Model 4] (i.e., AUCModel1 - AUCModel2, AUCModel1 - AUCModel3, AUCModel1 - AUCModel4) across 1000 bootstrap iterations. The difference in AUC was computed considering both mortality and severity as the outcome.

ELLA Cytokine panel

The ELLA platform is a method for rapid cytokine measurement using microfluidics ELISA assays. The assay measured TNF-α, IL-6, IL-8, and IL-1β, previously validated by the Mount Sinai Human Immune Monitoring Center (HIMC) using plasma from multiple myeloma patients and recently reported for large cohort of COVID-19 patients admitted to Mount Sinai Hospital[35].

Multiplexed proteomic assay (Olink)

For analysis of circulating cytokines, we used a multiplexed proteomic inflammation panel (Olink), which consists of 92 inflammation-related proteins quantified by an antibody-mediated proximity extension-based assay[89]. Samples with normalized protein expression values below the limit-of-detection in >75% of samples were excluded from further analysis. For the remainder of analytes, any sample under the limit of detection was assigned a value of the limit-of-detection divided by the square root of 2. The log2 fold-change over the median healthy control protein expression was then calculated, and the Benjamini-Hochberg[90] procedure was used to adjust P values for multiple testing

Consensus Clustering of Olink Data

For this analysis, we considered 238 samples with GI symptoms annotation. Consensus clustering was performed based on the abundance of 92 cytokines across all 238 samples. Consensus clustering was performed using the R packages ConsensusClusterPlus[91] based on z-score normalized data. Specifically, markers were partitioned into six clusters using the Kaplan

Meier (KM) algorithm, which was repeated 1000 times. Then, markers in each cluster were considered in order to derive cluster z-score signatures via package GSVA[92]. Based on these signatures, the association between different clusters and GI symptoms were derived via logistic regression with outcome corresponding to each GI symptom. **Fig. 2c** shows the signed FDR (-log10 scale). P-values were adjusted via Benjamini-Hochberg[90].

Defining associations between GI symptoms and Olink protein markers

Associations between GI symptoms and Olink proteomic data were derived using unpaired t-test comparing the symptomatic and asymptomatic groups. P-values were adjusted via Benjamini-Hochberg[90]. Only associations passing a 10% FDR were reported as significant (**Fig. 2d**).

Defining associations between GI symptoms and ELLA cytokine markers

Unpaired t-test were used to compare individual cytokines quantified by the ELLA panel between GI symptomatic and asymptomatic groups. P-values were adjusted via Benjamini-Hochberg[90].

Biopsy collection and processing for Mass cytometry (CyTOF)

Endoscopic biopsies were obtained from COVID-19 patients and non-COVID-19 controls during clinically indicated endoscopic procedures. The biopsies were processed in biosafety level 3 (BSL-3) facility within 2 hours of collection.

Briefly, biopsies were transferred to 10 ml of 'dissociation buffer' (1M HEPES(Lonza), 5uM EDTA(Invitrogen), 10% FBS in HBSS buffer (Gibco). The tubes were kept in a shaker (180 rpm, 37°C) for 20 min and then gently vortexed for 10 seconds. Cell suspensions were collected after passing the biopsies through 100um cell strainers. A second round of EDTA dissociation was performed as detailed above. The cell suspension was centrifuged at 1800 rpm for 10 min to pellet the epithelial fraction and kept on ice. The 'non-epithelial fraction' of the tissue was transferred to fresh tubes containing a 'digestion buffer' (2% FBS, 0.005g Collagenase type IV per sample (Sigma), 100 ul DNAse-I(Sigma) in 10ml in RPMI). Tubes were placed in the shaker (180 rpm, 37°C) for 40 min and thereafter gently vortexed for 30 sec. The digested tissues were filtered through 100 um cell strainers followed by a second round of filtration through 40um cell strainers. Cell suspensions were centrifuged at 1800 rpm for 10 min to obtain lamina propria mononuclear cells. Both epithelial cell (EC) and lamina propria (LP) pellets were then resuspended into 500ul of RPMI (Gibco) containing 10% FBS+ 1μlRh103 +1μl IdU and incubated at 37°C for 20 min. 5 ml RPMI (+10%FBS) was added to each tube and spun at 1800 rpm to pellet cells. 700μl of Prot1 stabilizer (SmartTube Inc.) was added to each tube and transferred to cryovials and incubated at

797 room temperature for 10 min. Cryovials were immediately transferred to -80 until the sample was
798 acquired for mass cytometry as detailed below.
799
800 **Blood collection and processing for CyTOF**
801 Phlebotomy was performed on COVID-19 patients and non-COVID-19 controls at the time of
802 endoscopic evaluation. All the blood samples from COVID-19 patients were processed in
803 enhanced BSL2 conditions per institutional guidelines. Briefly, 15ml of Lymphosep® -
804 Lymphocyte Separation Medium (MP Bio.) was added to each 50 ml centrifugation tube. Blood
805 was diluted with PBS to bring the volume up to 30ml and diluted blood was layered gently over
806 Lymphosep®. Tubes were then centrifuged at 2000 rpm for 20 mins with the brakes and
807 acceleration off. After centrifugation, with a 3ml transfer pipet, the buffy coat containing PBMCs
808 was transferred to another 15ml Falcon tube and was centrifuged at 1800 rpm for 10 mins. Pellets
809 were resuspended in PBS and tubes were centrifuged at 1800 rpm for 10 mins. PBMC pellets
810 were resuspended in the freezing medium (10% DMSO + 44% FBS in RPMI) and cryopreserved
811 at -80 °C.
812
813 **CyTOF processing and data acquisition**
814 Cells were processed and as previously described[93] according to the manufacturer's instructions.
815 Briefly, EC and LP SmartTube proteomic stabilized samples were thawed in a 10°C water bath
816 and washed with Cell Staining Buffer (Fluidigm). To facilitate data acquisition and doublet
817 removal, multiple samples were also barcoded using Fluidigm Pd barcoding kits and then washed
818 and pooled for data acquisition. Immediately prior to data acquisition, samples were washed with
819 Cell Staining Buffer and Cell Acquisition Solution (Fluidigm) and resuspended at a concentration
820 of 1 million cells per ml in Cell Acquisition Solution containing a 1:20 dilution of EQ Normalization
821 beads (Fluidigm). The samples were then acquired on a Helios Mass Cytometer equipped with a
822 wide-bore sample injector at an event rate of <400 events per second. After acquisition, repeat
823 acquisitions of the same sample concatenated and normalized using the Fluidigm software, and
824 barcoded samples were de-multiplexed using the Zunder single cell debarcoder.
825
826 **CyTOF Data analysis**
827 De-barcoded files were uploaded to Cytobank for analyses. Immune cells were identified based
828 on Ir-193 DNA intensity and CD45 expression; Ce140+ normalization beads, CD45-low/Ir-193-
829 low debris and cross-sample and Gaussian ion-cloud multiplets were excluded from subsequent
830 downstream analysis. Major immune cell types were identified using automated Astrolabe

approach, the result of which largely correlated well with our manual gating approaches. The impact of each tested condition on relative staining quality was evaluated in two ways: 1) overall correlations were determined by calculating the Pearson's correlation coefficients for the median expression of each marker across each defined immune subset; and 2) a staining index was calculated using defined populations showing the highest and lowest expression levels of each marker: SI = (Medianpos - Medianneg) / 2 X Std.Devneg. It is already shown that SmartTube-based fixation protocols take into account previously described mass cytometry artifacts such as cell-cell multiplets, isotopic spillover or oxidation, or mass cytometer instrument configuration[93].

Statistical Analysis for CyTOF

Pre-gated viable CD45+ cells were first clustered and annotated using the Astrolabe Cytometry Platform (Astrolabe Diagnostics, Inc.), which involves using a hierarchy-based FlowSOM algorithm for labeling cell populations in individual samples. These Astrolabe Profiling clusters from each tissue type were then meta-clustered across all samples utilizing Clustergrammer2's interactive heatmap as a method to interrogate antibody expression across every cluster and curate and assign cell population categories. Single sample clusters were also visualized using UMAP. Pairwise comparisons were performed on the frequencies of each identified cell population between the patient cohorts (COVID-19 vs. control, COVID-19 severe vs. control, COVID19-moderate vs. control) to determine fold change, p-values and FDR adjusted p-values using the Benjamini-Hochberg[90] method to account for multiple comparisons.

Cell Culture Experiments/ RNA isolation/ qPCR/Virus Isolation

African green monkey kidney epithelial cells (Vero E6) were originally purchased from American Type Culture Collection (ATCC). Cells were maintained in Dulbecco's modified Eagle's medium (DMEM) w/ L-glutamate, sodium pyruvate (Corning) supplemented with 10% fetal bovine serum (FBS), 100 U penicillin per ml, and 100 mg streptomycin per ml. For all experiments, the cells were always maintained in monolayers.

Several attempts were made to isolate live infectious particles from these biopsies. Briefly, biopsies were collected and stored in PBS until homogenization. Following homogenization and centrifugation (10,000 × g, 20 min, 4°C), the resulting supernatant tissue supernatant was inoculated onto Vero E6 monolayer maintained in optimal virus growth media for SARS-CoV-2 virus (DMEM w/ L-Glutamate, Sodium Pyruvate, 2% FBS, 100 U Penicillin/ml, and 100 mg Streptomycin/ml, 10 mM Non-Essential Amino Acids, 1 mM Sodium Pyruvate and 10 mM

HEPES). Vero E6 cells were incubated at 37 °C, 5% CO2 for a week and monitored daily for potential cytopathic effect (CPE).

Cell culture supernatants were also collected and assessed for presence of infective particles by plaque assay. Briefly, ten-fold serial dilutions were performed in infection media for SARS-CoV-2 and inoculated onto confluent Vero E6 cell monolayer in 6-well plate. After one-hour adsorption, supernatants were removed, and cells monolayers were overlaid with minimum essential media (MEM) containing 2% FBS and purified agar (OXOID) at a final concentration of 0.7%. Cells were then incubated 3 days at 37°C. Cells were fixed overnight with 10% formaldehyde for inactivation of potential SARS CoV2 virus. Overlay was removed and cells were washed once with PBS. A 2% crystal violet solution was used for plaque visualization and count. Experiments were performed under BSL3 conditions.

Specimen Processing for Nucleic Acid Extraction

Whole biopsy tissues from COVID-19 patients and non COVID controls were directly homogenized in Trizol (Invitrogen) and used to detect the presence of viral RNA. In parallel, RNA isolated from epithelial compartment and lamina propria fractions from biopsies post-processing were used for transcriptomics analyses. Total RNA was extracted using Direct-zol RNA Miniprep Plus (Zymo) kit according to the manufacturer's instructions.

RT-qPCR for Viral Determination

RNA was retro-transcribed using the enzyme Maxima First Strand cDNA (Thermofisher), and PCR reaction was performed using the TaqMan™ Universal PCR Master Mix (Thermofisher). For detection of SARS-CoV-2 RNA, we used the following primers and probe targeting the N gene:

N1- SARS-CoV2-F5'GACCCCAAAATCAGCGAAAT;

N1-SARS-CoV2-R5'TCTGGTTACTGCCAGTTGAATCTG;

N1-SARS-CoV2-P FAM5' ACCCCGCATTACGTTTGGTGGACC-BHQ-1 (https://www.cdc.gov/coronavirus/2019-ncov/lab/rt-pcr-panel-primer-probes.html)

Another set of primers was included to detect host 18s and GADPH. Limit of detection and amplification efficiency were calculated before GI tissue quantification for N1 (173%; R^2>0.94) primers using plasmids expressing the NP protein (2019-nCoV_N_Positive Control, IDT, cat. 10006625). RNA from GI tissue were run in triplicate in 384 plates using the following cycling conditions on the Roche LightCycler 480 Instrument II (Roche Molecular Systems, 05015243001): 50 C for 2 min; 95 C for 10 min; 40 cycles of 95C for 15 sec and 60 C for 1 min. Samples below the limit of detection (Ct≥34 corresponding to 100 genome copies/reaction) were considered

898 negative. Primers and probes for housekeeping genes GAPDH (assay ID Hs02758991_g1 FAM)
899 and 18S (assay ID Hs03928990_g1 FAM) were obtained from Thermofisher Scientific).
900
901 **Cell Culture Experiments/ Virus Isolation**
902 African green monkey kidney epithelial cells (Vero E6) were originally purchased from American
903 Type Culture Collection (ATCC). Cells were maintained in Dulbecco's modified Eagle's medium
904 (DMEM) w/ L-glutamate, sodium pyruvate supplemented with 10% fetal bovine serum (FBS), 100
905 U penicillin per ml, and 100 mg streptomycin per ml. For all experiments, the cells were always
906 maintained in monolayers.
907 Several attempts were made to isolate live infectious particles from these biopsies. Briefly,
908 biopsies were collected and stored in PBS until homogenization. Following homogenization and
909 centrifugation (10,000 × g, 20 min, 4°C), the resulting supernatant tissue supernatant was
910 inoculated onto Vero E6 monolayer maintained in optimal virus growth media for SARS-CoV-2
911 virus (DMEM w/ L-Glutamate, Sodium Pyruvate, 2% FBS, 100 U Penicillin/ml, and 100 mg
912 Streptomycin/ml, 10 mM Non-Essential Amino Acids, 1 mM Sodium Pyruvate and 10 mM
913 HEPES). Vero E6 cells were incubated at 37 °C, 5% CO2 for a week and monitored daily for
914 potential cytopathic effect (CPE).
915 Cell culture supernatants were also collected and assessed for presence of infective
916 particles by plaque assay. Briefly, ten-fold serial dilutions were performed in infection media for
917 SARS-CoV-2 and inoculated onto confluent Vero E6 cell monolayer in 6-well plate. After one-hour
918 adsorption, supernatants were removed, and cells monolayers were overlaid with minimum
919 essential media (MEM) containing 2% FBS and purified agar (OXOID) at a final concentration of
920 0.7%. Cells were then incubated 3 days at 37°C. Cells were fixed overnight with 10%
921 formaldehyde for inactivation of potential SARS CoV2 virus. Overlay was removed and cells were
922 washed once with PBS. A 2% crystal violet solution was used for plaque visualization and count.
923 Experiments were performed under BSL3 conditions.
924
925 **RNA Sequencing**
926
927 *Library preparation and sequencing*
928 RNA-sequencing (RNA-seq) was performed on tissue biopsies from paired EC and LP samples
929 from COVID-19 cases and controls. Directional RNA-seq libraries were prepared from 50 ng of
930 total RNA with the TruSeq® Stranded Total RNA prep with Ribo-Zero kit (cat no. 20020599).

Paired-end (100 bp) sequencing was performed for DNA libraries on an Illumina NovaSeq instrument on a NovaSeq S1 Flowcell, with an average yield of 39 million PE reads/sample.

RNA-seq analysis

Base-calling and quality scoring of sequencing data were done through Illumina's Real-Time Analysis (RTA) software. RNA-seq data processing and reference mapping were done with custom analysis scripts combining publicly available tools as previously described[94] with modifications as follows, reads were mapped to a custom reference that combined the human hg38 reference genome (Release 34, GRCh38.p13) and the SARS-CoV-2 genome (RefSeq NC_045512) for simultaneous quantification of host and virus transcripts.

Differential gene expression (DGE) analysis was performed with the Bioconductor edgeR package [95] using as input a combined matrix of mapped paired-end read raw counts, with genes in rows and samples in columns. Prior to DEG analysis, gene counts were converted to fragments per kb per million reads (FPKM) with the RSEM package with default settings in strand-specific mode[96].

Genes with less than 1 FPKM in at least 50% of the samples were removed. The remaining gene counts were then normalized across samples using the weighted trimmed mean of M-values (TMM) method[97].The dispersion was estimated by fitting a generalized linear model (GLM) as implemented in edgeR, sex was fitted as a covariate on a per-patient paired design. Pairwise comparisons were performed between sample groups (i.e., between tissue sections, and between cases and controls). Significant expression differences were selected based on eBayes adjusted p values corrected for multiple testing using the Benjamini-Hochberg method ($q \leq 0.05$).

Gene Ontology and Pathway Enrichment Analysis

KEGG pathway and gene ontology (GO) biological process (BP), molecular function (MF), and/or cellular component (CC) enrichment analyses were performed using the gProfileR R v0.6.8 package[98]. The background gene set was restricted genes with detected expression (defined as genes with expression levels above 1 FPKM in at least 50% of samples). Genes with differential expression were ranked by log 2 fold change and used as an ordered query. P values were corrected using the g:SCS algorithm to account for multiple comparisons.

Cell-type deconvolution and gene signature enrichment analysis

For cell-type deconvolution of the bulk RNA-seq data, gene set enrichment analysis of differentially expressed genes of cases vs controls comparisons was performed against cell type

gene-expression single-cell signatures from intestinal mucosa[46] and dendritic cell (DCs) subsets gene-expression signatures from ileum[45]. Similarly, differentially expressed genes were tested for enrichment of gene signatures associated with an antiviral response, inflammation, and cytokine signaling in acutely infected post-mortem tissue with SARS-CoV-2[30] , were tested for significant ($p \leq 0.05$) enrichment using Fisher's exact tests and using Bonferroni correction for multiple comparisons.

Additionally, Geneset enrichment analysis (GSEA)[99] was carried out on a rank ordered list of the infected EC versus control molecular analysis. The ranking metric used was logFC * -logP value, however, the results were similar when logFC metric was also used (data not shown). For the COVID-19 associated datasets we curated two signatures from infected organoids[100]: hSIOs-COVID-19: human small intestinal organoids (hSIOs) grown in either i) Wnt high expansion (EXP) medium (at adjP<0.05) or ii) differentiation (DIF) medium (at adjP<0.1). The standard GSEA settings were used, namely 'meandiv' for normalization mode, 'weighted' enrichment statistic, and '1000' permutations. GSEA using the Hallmark database (v7.1, [101]) was also performed with the same settings.

Immunofluorescent (IF) microscopy

Formalin fixed, paraffin embedded tissue acquired during routine clinical care was obtained from the pathology core at our institution. Sections (5μm) were dewaxed in xylene and rehydrated in graded alcohol and then phosphate-buffered saline (PBS). Heat-induced epitope retrieval was performed by incubating slides in a pressure cooker for 15 minutes on high in target retrieval solution (Dako, S1699). Slides were then left to cool in the solution at room temperature for 30 minutes. Slides were washed twice in PBS and then permeabilized for 30 minutes in 0.1% tritonX-100 in PBS. Non-specific binding was blocked with 10% goat serum for 1 hour at room temperature. Sections were then incubated in primary antibodies diluted in blocking solution overnight at 4°C. Primary and secondary antibodies are summarized in **Supplementary Table 11**. Slides were washed in PBST (0.1% tween 20, PBS) 3 times and then incubated in secondary antibody and 4′,6-diamidino-2-phenylindole (1ug/mL) for 1 hour at room temperature. Sections were washed twice in PBST and once in PBS then mounted with Fluoromount-G (Electron microscopy sciences, 1798425). Controls included, omitting primary antibody (no primary control), or substituting primary antibodies with non-reactive antibodies of the same isotype (isotype control). Tissue was visualized and imaged using a Nikon Eclipse Ni microscope and digital SLR camera (Nikon, DS-Qi2).

Electron Microscopy (EM)

Biopsy specimens for electron microscopy were placed in 3% buffered glutaraldehyde. Following post-fixation in 1% osmium tetroxide, tissues were serially dehydrated and embedded in epoxy resin in standard fashion. One-micron toluidine-stained scout sections were prepared for light microscopic orientation; 80nm ultrathin sections for EM were stained with uranyl acetate and lead citrate and examined in a Hitachi 7650 transmission electron microscope at 80kV.

Acknowledgements

We would like to thank the clinical staff, physicians and patients who participated in this study. This research was partly funded by NIH/NIDDK123749 (SM). Additional support was provided by CRIP (Center for Research for Influenza Pathogenesis), a NIAID supported Center of Excellence for Influenza Research and Surveillance (CEIRS, contract # HHSN272201400008C), and NIAID R01AI113186 (to H.B). Additionally, the work was supported by the generous support of the JPB Foundation, the Open Philanthropy Project (research grant 2020-215611 (5384)), the Defense Advanced Research Projects Agency, and anonymous donors to AG-S. MT was funded by the Digestive Disease Research Foundation (DDRF). A.S.G-R. is supported in part by a Robin Chemers Neustein Postdoctoral Fellowship Award. The research carried out by H.V.B and A.S.G-R was supported by the Office of Research Infrastructure of the National Institutes of Health (NIH) under awards S10OD018522 and S10OD026880. S.T.C. is supported by grant F30CA243210. G.J.B. is supported by a Research Fellowship Award from the Crohn's and Colitis Foundation of America. M.P.S. is supported by NIH T32 5T32AI007605. S.G. is supported by grants U24 CA224319, U01 DK124165, and P01 CA190174. We also thank Randy Albrecht for support with the BSL3 facility and procedures at the Icahn School of Medicine at Mount Sinai (ISMMS).

References

1. Zhu, N.*, et al.* A Novel Coronavirus from Patients with Pneumonia in China, 2019. *N Engl J Med* **382**, 727-733 (2020).
2. Wang, C., Horby, P.W., Hayden, F.G. & Gao, G.F. A novel coronavirus outbreak of global health concern. *Lancet* **395**, 470-473 (2020).
3. Huang, C.*, et al.* Clinical features of patients infected with 2019 novel coronavirus in Wuhan, China. *Lancet* **395**, 497-506 (2020).
4. Goyal, P.*, et al.* Clinical Characteristics of Covid-19 in New York City. *N Engl J Med* **382**, 2372-2374 (2020).

5. Xu, T., *et al.* Epidemiological and clinical features of asymptomatic patients with SARS-CoV-2 infection. *J Med Virol* (2020).
6. Coronavirus Disease 2019 (COVID-19): Symptoms of Coronavirus: Centers for Disease Control and Prevention, 2020. https://www.cdc.gov/coronavirus/2019-ncov/symptoms-testing/symptoms.html. Last updated May 13, 2020.
7. Jin, X., *et al.* Epidemiological, clinical and virological characteristics of 74 cases of coronavirus-infected disease 2019 (COVID-19) with gastrointestinal symptoms. *Gut* **69**, 1002-1009 (2020).
8. Pan, L., *et al.* Clinical Characteristics of COVID-19 Patients With Digestive Symptoms in Hubei, China: A Descriptive, Cross-Sectional, Multicenter Study. *Am J Gastroenterol* **115**, 766-773 (2020).
9. Gupta, A., *et al.* Extrapulmonary manifestations of COVID-19. *Nat Med* **26**, 1017-1032 (2020).
10. Tian, Y., Rong, L., Nian, W. & He, Y. Review article: gastrointestinal features in COVID-19 and the possibility of faecal transmission. *Aliment Pharmacol Ther* **51**, 843-851 (2020).
11. Cheung, K.S., *et al.* Gastrointestinal Manifestations of SARS-CoV-2 Infection and Virus Load in Fecal Samples From a Hong Kong Cohort: Systematic Review and Meta-analysis. *Gastroenterology* **159**, 81-95 (2020).
12. Harmer, D., Gilbert, M., Borman, R. & Clark, K.L. Quantitative mRNA expression profiling of ACE 2, a novel homologue of angiotensin converting enzyme. *FEBS Lett* **532**, 107-110 (2002).
13. Suárez-Fariñas, M., *et al.* Intestinal inflammation modulates the expression of ACE2 and TMPRSS2 and potentially overlaps with the pathogenesis of SARS-CoV-2 related disease. *bioRxiv*, 2020.2005.2021.109124 (2020).
14. Young, B.E., *et al.* Epidemiologic Features and Clinical Course of Patients Infected with SARS-CoV-2 in Singapore. *JAMA - Journal of the American Medical Association* (2020).
15. Xiao, F., *et al.* Evidence for Gastrointestinal Infection of SARS-CoV-2. *Gastroenterology* **158**, 1831-1833 e1833 (2020).
16. Holshue, M.L., *et al.* First Case of 2019 Novel Coronavirus in the United States. *N Engl J Med* **382**, 929-936 (2020).
17. Wu, Y., *et al.* Prolonged presence of SARS-CoV-2 viral RNA in faecal samples. *Lancet Gastroenterol Hepatol* **5**, 434-435 (2020).
18. Fehr, A.R. & Perlman, S. Coronaviruses: An overview of their replication and pathogenesis. (2015).
19. Leung, W.K., *et al.* Enteric involvement of severe acute respiratory syndrome-associated coronavirus infection. *Gastroenterology* **125**, 1011-1017 (2003).
20. Chan, K.H., *et al.* Detection of SARS coronavirus in patients with suspected SARS. *Emerg Infect Dis* **10**, 294-299 (2004).
21. Assiri, A., *et al.* Epidemiological, demographic, and clinical characteristics of 47 cases of Middle East respiratory syndrome coronavirus disease from Saudi Arabia: a descriptive study. *Lancet Infect Dis* **13**, 752-761 (2013).
22. Corman, V.M., *et al.* Detection of 2019 novel coronavirus (2019-nCoV) by real-time RT-PCR. *Euro Surveill* **25**(2020).

23. Wang, X., *et al.* Aberrant gut microbiota alters host metabolome and impacts renal failure in humans and rodents. *Gut* (2020).
24. Sultan, S., *et al.* AGA Institute Rapid Review of the GI and Liver Manifestations of COVID-19, Meta-Analysis of International Data, and Recommendations for the Consultative Management of Patients with COVID-19. *Gastroenterology* (2020).
25. Munster, V.J., *et al.* Respiratory disease in rhesus macaques inoculated with SARS-CoV-2. *Nature* (2020).
26. Bojkova, D., *et al.* Proteomics of SARS-CoV-2-infected host cells reveals therapy targets. *Nature* (2020).
27. Zang, R., *et al.* TMPRSS2 and TMPRSS4 promote SARS-CoV-2 infection of human small intestinal enterocytes. *Sci Immunol* **5**(2020).
28. Zhou, J., *et al.* Infection of bat and human intestinal organoids by SARS-CoV-2. *Nat Med* (2020).
29. Lamers, M.M., *et al.* SARS-CoV-2 productively infects human gut enterocytes. *Science* (2020).
30. Blanco-Melo, D., *et al.* Imbalanced Host Response to SARS-CoV-2 Drives Development of COVID-19. *Cell* **181**, 1036-1045 e1039 (2020).
31. Lucas, C., *et al.* Longitudinal analyses reveal immunological misfiring in severe COVID-19. *Nature* **584**, 463-469 (2020).
32. Xu, X., *et al.* Analysis of inflammatory parameters and disease severity for 88 hospitalized COVID-19 patients in Wuhan, China. *Int J Med Sci* **17**, 2052-2062 (2020).
33. Liu, Z., *et al.* Dynamic Interleukin-6 Level Changes as a Prognostic Indicator in Patients With COVID-19. *Front Pharmacol* **11**, 1093 (2020).
34. Akbari, H., *et al.* The role of cytokine profile and lymphocyte subsets in the severity of coronavirus disease 2019 (COVID-19): A systematic review and meta-analysis. *Life Sci* **258**, 118167 (2020).
35. Del Valle, D.M., *et al.* An inflammatory cytokine signature helps predict COVID-19 severity and death. *medRxiv* (2020).
36. Laing, A.G., *et al.* A dynamic COVID-19 immune signature includes associations with poor prognosis. *Nat Med* (2020).
37. Mathew, D., *et al.* Deep immune profiling of COVID-19 patients reveals distinct immunotypes with therapeutic implications. *Science* (2020).
38. Liu, J., *et al.* Longitudinal characteristics of lymphocyte responses and cytokine profiles in the peripheral blood of SARS-CoV-2 infected patients. *EBioMedicine* **55**, 102763 (2020).
39. Arunachalam, P.S., *et al.* Systems biological assessment of immunity to mild versus severe COVID-19 infection in humans. *Science* (2020).
40. Richardson, S., *et al.* Presenting Characteristics, Comorbidities, and Outcomes Among 5700 Patients Hospitalized With COVID-19 in the New York City Area. *JAMA* (2020).
41. Team, C.C.-R. Severe Outcomes Among Patients with Coronavirus Disease 2019 (COVID-19) - United States, February 12-March 16, 2020. *MMWR Morb Mortal Wkly Rep* **69**, 343-346 (2020).
42. Falschlehner, C., Schaefer, U. & Walczak, H. Following TRAIL's path in the immune system. *Immunology* **127**, 145-154 (2009).

43. Chyuan, I.T., Tsai, H.F., Wu, C.S., Sung, C.C. & Hsu, P.N. TRAIL-Mediated Suppression of T Cell Receptor Signaling Inhibits T Cell Activation and Inflammation in Experimental Autoimmune Encephalomyelitis. *Front Immunol* **9**, 15 (2018).
44. Mackall, C.L., Fry, T.J. & Gress, R.E. Harnessing the biology of IL-7 for therapeutic application. *Nat Rev Immunol* **11**, 330-342 (2011).
45. Martin, J.C.*, et al.* Single-Cell Analysis of Crohn's Disease Lesions Identifies a Pathogenic Cellular Module Associated with Resistance to Anti-TNF Therapy. *Cell* **178**, 1493-1508 e1420 (2019).
46. Smillie, C.S.*, et al.* Intra- and Inter-cellular Rewiring of the Human Colon during Ulcerative Colitis. *Cell* **178**, 714-730 e722 (2019).
47. Kotarsky, K.*, et al.* A novel role for constitutively expressed epithelial-derived chemokines as antibacterial peptides in the intestinal mucosa. *Mucosal Immunol* **3**, 40-48 (2010).
48. Hamming, I.*, et al.* Tissue distribution of ACE2 protein, the functional receptor for SARS coronavirus. A first step in understanding SARS pathogenesis. *Journal of Pathology* (2004).
49. Li, M.Y., Li, L., Zhang, Y. & Wang, X.S. Expression of the SARS-CoV-2 cell receptor gene ACE2 in a wide variety of human tissues. *Infect Dis Poverty* **9**, 45 (2020).
50. Nobel, Y.R.*, et al.* Gastrointestinal Symptoms and Coronavirus Disease 2019: A Case-Control Study From the United States. *Gastroenterology* **159**, 373-375 e372 (2020).
51. Blumfield, E. & Levin, T.L. COVID-19 in pediatric patients: a case series from the Bronx, NY. *Pediatr Radiol* (2020).
52. Blumfield, E., Levin, T.L., Kurian, J., Lee, E.Y. & Liszewski, M.C. Imaging Findings in Multisystem Inflammatory Syndrome in Children (MIS-C) Associated with COVID. *AJR Am J Roentgenol* (2020).
53. Aghemo, A.*, et al.* COVID-19 Digestive System Involvement and Clinical Outcomes in a Large Academic Hospital in Milan, Italy. *Clin Gastroenterol Hepatol* (2020).
54. Lin, L.*, et al.* Gastrointestinal symptoms of 95 cases with SARS-CoV-2 infection. *Gut* **69**, 997-1001 (2020).
55. Mehta, P.*, et al.* COVID-19: consider cytokine storm syndromes and immunosuppression. *Lancet* **395**, 1033-1034 (2020).
56. Cao, W.*, et al.* High-Dose Intravenous Immunoglobulin as a Therapeutic Option for Deteriorating Patients With Coronavirus Disease 2019. *Open Forum Infect Dis* **7**, ofaa102 (2020).
57. Cavalli, G.*, et al.* Interleukin-1 blockade with high-dose anakinra in patients with COVID-19, acute respiratory distress syndrome, and hyperinflammation: a retrospective cohort study. *Lancet Rheumatol* **2**, e325-e331 (2020).
58. Guo, Y.-R.*, et al.* The origin, transmission and clinical therapies on coronavirus disease 2019 (COVID-19) outbreak – an update on the status. *Military Medical Research* (2020).
59. Ackermann, M.*, et al.* Pulmonary Vascular Endothelialitis, Thrombosis, and Angiogenesis in Covid-19. *N Engl J Med* **383**, 120-128 (2020).
60. Zhang, H.*, et al.* Histopathologic Changes and SARS-CoV-2 Immunostaining in the Lung of a Patient With COVID-19. *Ann Intern Med* **172**, 629-632 (2020).

61. Cheng, Y.*, et al.* Kidney disease is associated with in-hospital death of patients with COVID-19. *Kidney Int* **97**, 829-838 (2020).
62. Gabarre, P.*, et al.* Acute kidney injury in critically ill patients with COVID-19. *Intensive Care Med* **46**, 1339-1348 (2020).
63. Varga, Z.*, et al.* Endothelial cell infection and endotheliitis in COVID-19. *Lancet* **395**, 1417-1418 (2020).
64. Liao, M.*, et al.* Single-cell landscape of bronchoalveolar immune cells in patients with COVID-19. *Nat Med* **26**, 842-844 (2020).
65. Bradley, B.T.*, et al.* Histopathology and ultrastructural findings of fatal COVID-19 infections in Washington State: a case series. *Lancet* **396**, 320-332 (2020).
66. Gaffen, S.L. Structure and signalling in the IL-17 receptor family. *Nat Rev Immunol* **9**, 556-567 (2009).
67. Miossec, P. & Kolls, J.K. Targeting IL-17 and TH17 cells in chronic inflammation. *Nat Rev Drug Discov* **11**, 763-776 (2012).
68. Wu, D. & Yang, X.O. TH17 responses in cytokine storm of COVID-19: An emerging target of JAK2 inhibitor Fedratinib. *J Microbiol Immunol Infect* **53**, 368-370 (2020).
69. Josset, L.*, et al.* Cell host response to infection with novel human coronavirus EMC predicts potential antivirals and important differences with SARS coronavirus. *mBio* **4**, e00165-00113 (2013).
70. Faure, E.*, et al.* Distinct immune response in two MERS-CoV-infected patients: can we go from bench to bedside? *PLoS One* **9**, e88716 (2014).
71. Ramirez-Carrozzi, V.*, et al.* IL-17C regulates the innate immune function of epithelial cells in an autocrine manner. *Nat Immunol* **12**, 1159-1166 (2011).
72. Pan, J.*, et al.* A novel chemokine ligand for CCR10 and CCR3 expressed by epithelial cells in mucosal tissues. *J Immunol* **165**, 2943-2949 (2000).
73. Girard, D., Paquet, M.E., Paquin, R. & Beaulieu, A.D. Differential effects of interleukin-15 (IL-15) and IL-2 on human neutrophils: modulation of phagocytosis, cytoskeleton rearrangement, gene expression, and apoptosis by IL-15. *Blood* **88**, 3176-3184 (1996).
74. Regamey, N.*, et al.* Airway epithelial IL-15 transforms monocytes into dendritic cells. *Am J Respir Cell Mol Biol* **37**, 75-84 (2007).
75. Mattei, F., Schiavoni, G., Belardelli, F. & Tough, D.F. IL-15 is expressed by dendritic cells in response to type I IFN, double-stranded RNA, or lipopolysaccharide and promotes dendritic cell activation. *J Immunol* **167**, 1179-1187 (2001).
76. Rojas, J.M., Avia, M., Martin, V. & Sevilla, N. IL-10: A Multifunctional Cytokine in Viral Infections. *J Immunol Res* **2017**, 6104054 (2017).
77. Han, H.*, et al.* Profiling serum cytokines in COVID-19 patients reveals IL-6 and IL-10 are disease severity predictors. *Emerg Microbes Infect* **9**, 1123-1130 (2020).
78. Diao, B.*, et al.* Reduction and Functional Exhaustion of T Cells in Patients With Coronavirus Disease 2019 (COVID-19). *Front Immunol* **11**, 827 (2020).
79. Laterre, P.F.*, et al.* Association of Interleukin 7 Immunotherapy With Lymphocyte Counts Among Patients With Severe Coronavirus Disease 2019 (COVID-19). *JAMA Netw Open* **3**, e2016485 (2020).
80. Strater, J.*, et al.* TRAIL and its receptors in the colonic epithelium: a putative role in the defense of viral infections. *Gastroenterology* **122**, 659-666 (2002).

81. Shi, H.*, et al.* Neutrophil calprotectin identifies severe pulmonary disease in COVID-19. *medRxiv* (2020).
82. Chu, H.*, et al.* Comparative replication and immune activation profiles of SARS-CoV-2 and SARS-CoV in human lungs: an ex vivo study with implications for the pathogenesis of COVID-19. *Clin Infect Dis* (2020).
83. Bost, P.*, et al.* Host-Viral Infection Maps Reveal Signatures of Severe COVID-19 Patients. *Cell* **181**, 1475-1488 e1412 (2020).
84. Chen, L.*, et al.* Elevated serum levels of S100A8/A9 and HMGB1 at hospital admission are correlated with inferior clinical outcomes in COVID-19 patients. *Cell Mol Immunol* (2020).
85. Pelaseyed, T.*, et al.* The mucus and mucins of the goblet cells and enterocytes provide the first defense line of the gastrointestinal tract and interact with the immune system. *Immunol Rev* **260**, 8-20 (2014).
86. Strober, W. & Fuss, I.J. Proinflammatory cytokines in the pathogenesis of inflammatory bowel diseases. *Gastroenterology* **140**, 1756-1767 (2011).
87. Strober, W., Fuss, I.J. & Blumberg, R.S. The immunology of mucosal models of inflammation. *Annu Rev Immunol* **20**, 495-549 (2002).
88. Chistiakov, D.A., Bobryshev, Y.V., Kozarov, E., Sobenin, I.A. & Orekhov, A.N. Intestinal mucosal tolerance and impact of gut microbiota to mucosal tolerance. *Front Microbiol* **5**, 781 (2014).
89. Gruber, C.*, et al.* Mapping Systemic Inflammation and Antibody Responses in Multisystem Inflammatory Syndrome in Children (MIS-C). *medRxiv* (2020).
90. Benjamini, Y. & Hochberg, Y. Controlling the False Discovery Rate: A Practical and Powerful Approach to Multiple Testing. *Journal of the Royal Statistical Society. Series B (Methodological)* **57**, 289-300 (1995).
91. Wilkerson, M.D. & Hayes, D.N. ConsensusClusterPlus: a class discovery tool with confidence assessments and item tracking. *Bioinformatics* **26**, 1572-1573 (2010).
92. Hanzelmann, S., Castelo, R. & Guinney, J. GSVA: gene set variation analysis for microarray and RNA-seq data. *BMC Bioinformatics* **14**, 7 (2013).
93. Geanon, D.*, et al.* A Streamlined CyTOF Workflow To Facilitate Standardized Multi-Site Immune Profiling of COVID-19 Patients. *medRxiv* (2020).
94. Holmes, G.*, et al.* Integrated Transcriptome and Network Analysis Reveals Spatiotemporal Dynamics of Calvarial Suturogenesis. *Cell Rep* **32**, 107871 (2020).
95. Robinson, M.D., McCarthy, D.J. & Smyth, G.K. edgeR: a Bioconductor package for differential expression analysis of digital gene expression data. *Bioinformatics* **26**, 139-140 (2010).
96. Li, B. & Dewey, C.N. RSEM: accurate transcript quantification from RNA-Seq data with or without a reference genome. *BMC Bioinformatics* **12**, 323 (2011).
97. Robinson, M.D. & Oshlack, A. A scaling normalization method for differential expression analysis of RNA-seq data. *Genome Biol* **11**, R25 (2010).
98. Reimand, J., Kull, M., Peterson, H., Hansen, J. & Vilo, J. g:Profiler--a web-based toolset for functional profiling of gene lists from large-scale experiments. *Nucleic Acids Res* **35**, W193-200 (2007).

99. Subramanian, A.*, et al.* Gene set enrichment analysis: a knowledge-based approach for interpreting genome-wide expression profiles. *Proc Natl Acad Sci U S A* **102**, 15545-15550 (2005).
100. Lamers, M.M.*, et al.* SARS-CoV-2 productively infects human gut enterocytes. *Science* **369**, 50-54 (2020).
101. Liberzon, A.*, et al.* The Molecular Signatures Database (MSigDB) hallmark gene set collection. *Cell Syst* **1**, 417-425 (2015).

Table 1: Basic demographics and clinical characteristics in patients with and without GI symptoms. Number patients (%). For age, an unpaired t-test was performed. For categorical variables, the Fisher's exact test or the Chi-square test was used as appropriate.

	Total (n=634)	**GI symptoms (n=299)**	**No GI symptoms (n=335)**	**p-value**
Age (years)	64.0 ± 15.7	60.5 ± 15.0	67.2 ± 15.7	**<0.0001**
Male	369 ± 58.2	168 ± 56.2	201 ± 60.0	0.33
Race/ethnicities				
Hispanic	177 ± 27.9	85 ± 28.4	92 ± 27.5	
African-American	161 ± 25.4	66 ± 22.1	95 ± 28.4	
White	137 ± 21.6	70 ± 23.4	67 ± 20.0	
Asian	35 ± 5.5	22 ± 7.4	13 ± 3.9	
Other	124 ± 19.6	56 ± 18.7	68 ± 20.3	0.13
Comorbidities				
HTN	229 ± 36.1	112 ± 37.5	117 ± 34.9	0.51
Diabetes	141 ± 22.2	58 ± 19.4	83 ± 24.8	0.13
Obesity (BMI>30)*	211 ± 37.1	108 ± 40.6	103 ± 34.1	0.12
Chronic lung disease	59 ± 9.3	34 ± 11.4	25 ± 7.5	0.10
Heart disease	111 ± 17.5	48 ± 16.1	63 ± 18.8	0.40
Chronic kidney disease	95 ± 15.0	41 ± 13.7	54 ± 16.1	0.44
Cancer	66 ± 10.4	27 ± 9.0	39 ± 11.6	0.30
HIV	11 ± 1.7	5 ± 1.7	6 ± 1.8	0.99
IBD	7 ± 1.1	4 ± 1.3	3 ± 0.9	0.71

*BMI information available on only 568 patients

Table 2: Disease severity and clinical outcomes in those with and without GI symptoms. The Fisher's exact test or the Chi-square test was used as appropriate.

Disease severity	**Total (n=634)**	**GI symptoms (n=299)**	**No GI symptoms (n=335)**	**p-value**
Mild	54 ± 8.5	31 ± 10.4	23 ± 6.9	
Moderate	361 ± 56.9	188 ± 62.9	173 ± 51.6	
Severe	158 ± 24.9	63 ± 21.1	95 ± 28.4	
Severe with EOD	61 ± 9.6	17 ± 5.7	44 ± 13.1	**0.0004**
ICU admission	110 ± 17.4	45 ± 15.1	65 ± 19.4	0.17
Mortality	151 ± 23.8	47 ± 15.7	104 ± 31.0	**<0.0001**

Table 3: Proportion of patients with GI symptoms

GI symptom	**Number patients (%)**
Nausea	157 ± 24.8
Vomiting	82 ± 12.9
Diarrhea	245 ± 38.6
Any GI symptom	299 ± 47.2

Table 4: Basic demographics in survivors and non-survivors. For age, an unpaired t-test was performed. For categorical variables, the Fisher's exact test or the Chi-square test was used as appropriate.

	Total (n=634)	**Survivors (n=483)**	**Non-survivors (n=151)**	**p-value**
Age (years)	64.0 ± 15.7	61.3 ± 15.2	72.6 ± 14.1	**<0.0001**
Male	369 (58.2)	287 (59.4)	82 (54.3)	0.30
Disease severity				
Mild	54 ± 8.5	48 ± 9.9	6 ± 4.0	
Moderate	361 ± 56.9	318 ± 65.8	43 ± 28.5	
Severe	158 ± 24.9	95 ± 19.7	63 ± 41.7	
Severe with EOD	61 ± 9.6	22 ± 4.6	39 ± 25.8	**<0.0001**

Table 5: Age, gender and mortality in an external validation (Italian) cohort stratified by presence or absence of diarrhea on admission. For age, an unpaired t-test was performed. For categorical variables, the Fisher's exact test or the Chi-square test was used as appropriate.

	Total (n=287)	**Diarrhea on admission (n=80)**	**No diarrhea on admission (n=207)**	**p-value**
Age (years)	64.2 ± 13.6	60.6 ± 13.9	65.5 ± 13.3	**0.0056**
Male	195 ± 67.9	46 ± 57.5	149 ± 72.0	**0.0238**
ICU admission	52 ± 18.1	9 ± 11.3	43 ± 20.8	0.06
Mortality	57 ± 19.9	8 ± 10.0	49 ± 23.7	**0.008**
Death or ICU admission	99 ± 34.5	16 ± 20.0	83 ± 40.1	**0.0014**

Table 6: Clinical characteristics of patients who underwent endoscopic GI biopsies

Patient #	Age*	Sex	Procedure	Tissue sample location	COVID-19 Antibody	Days from symptom onset (or first SARS-CoV-2 PCR if asymptomatic) to procedure	Days from last positive SARS-CoV-2 PCR to procedure (0 if positive swab after procedure)	COVID severity on admission
1	60-65	M	EGD	Duodenum	NA	10	10	Severe with EOD
2	5-10	M	EGD & colonoscopy	Intestinal Transplant	Positive	23	0	Severe
3	75-80	M	EGD	Duodenum	NA	25	9	Mild
4	30-35	F	EGD	Duodenum	NA	44	31	Severe with EOD
5	60-65	M	EGD	Duodenum	Positive	24	NA	Moderate
6	50-55	M	EGD	Duodenum	Positive	11	0	Asymptomatic / mild
7	55-60	M	EGD	Duodenum	Positive	19	19	Asymptomatic / mild
8	65-70	F	EGD	Duodenum	Positive	30	23	Severe
9	75-80	M	EGD	Duodenum	Positive	24	0	Severe
*10***	*80-85*	*F*	*EGD*	*Duodenum*	*NA*	*NA*	*NA*	*NA*
11	90-95	F	EGD	Duodenum	Positive	36	0	Severe with EOD
12	50-55	F	Colonoscopy	Ileum	NA	37	31	Mild
13	40-45	M	EGD	Duodenum	Positive	18	0	Mild
14	65-70	F	EGD	Duodenum	Positive	37	32	Severe with EOD
15	30-35	F	EGD	Duodenum	Positive	50	48	Mild
16	70-75	F	EGD	Duodenum	Positive	25	19	Mild
17	50-55	M	EGD	Duodenum	NA	52	52	Mild
18	35-40	M	EGD	Duodenum	NA	3	3	Asymptomatic / mild

* Age is provided as a range to obscure identifying information related to individuals

**Patient 10 was excluded from analysis because SARS-CoV-2 nasopharyngeal PCR testing was repeatedly negative and her COVID-19 antibodies were also negative. Her inclusion initially was based on an atypical pulmonary infiltrate on chest X-ray and a viral syndrome in two of her family members.

Fig. 1: GI symptoms in COVID-19 patients associated with reduced severity and mortality

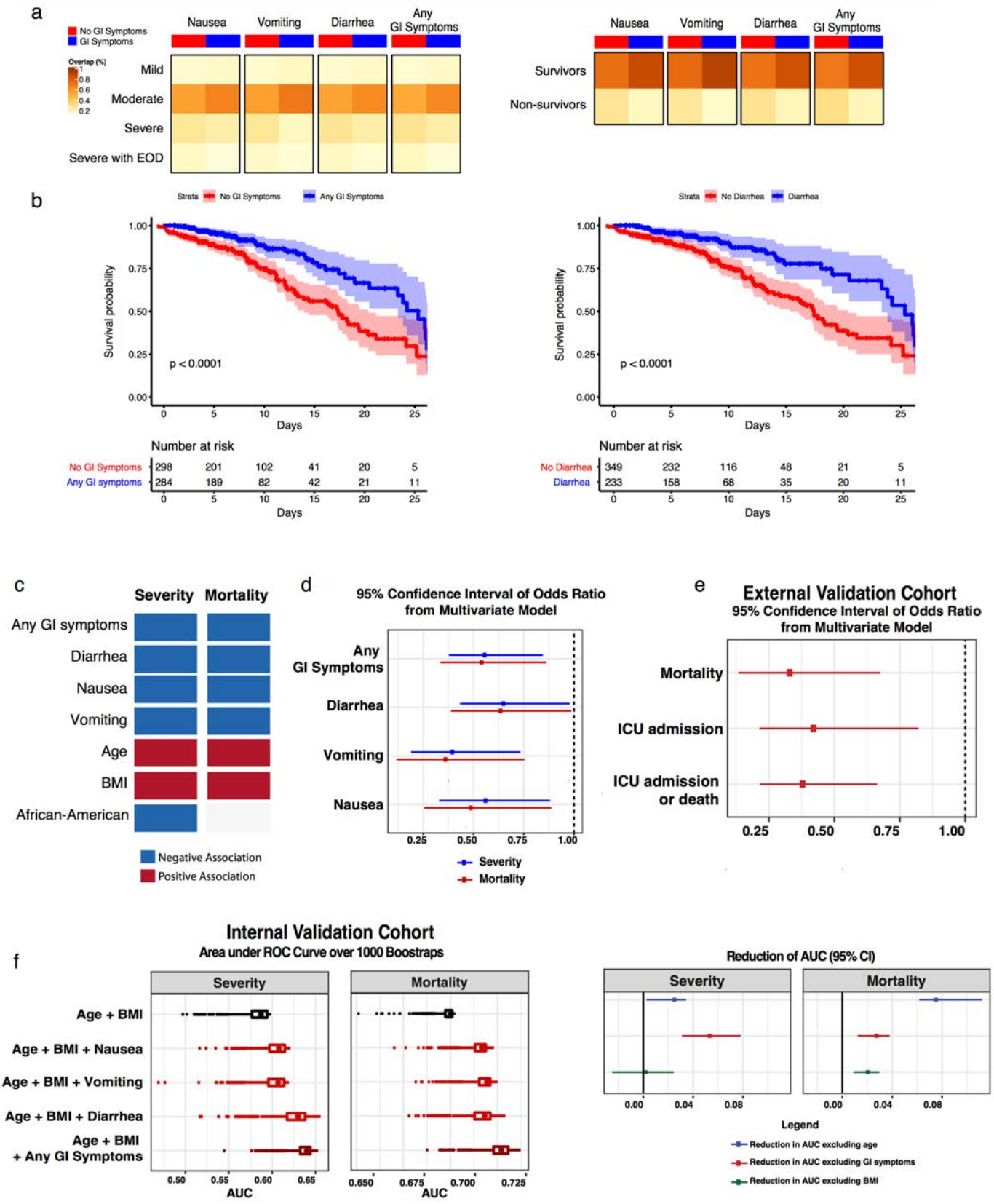

a, Inverse association between GI symptoms (nausea, vomiting, diarrhea, and any GI symptoms) with severity and mortality in the discovery cohort. For each GI symptom (columns), the percentage of patients allocated (as indicated by % overlap) to severity and mortality status (rows) is displayed. P-values from Fisher-Exact test for the association between GI symptoms and severity (less than 0.001) or mortality (less than 0.05). **b,** Kaplan-Meier (KM) curves for survival stratified by any GI Symptoms (left panel) and diarrhea (right panel) for patients in the Discovery Cohort. P-values from log-rank test and 95% confidence intervals of KM curves are shown. Below each KM curve, the number of patients at risk are reported for the respective time points. **c,** Significant variables associated with mortality and severity in multivariate logistic regression. Significant associations were derived via 95% confidence intervals based on 1000 bootstrap iterations. Negative associations are displayed in blue; while positive associations in red. Severity and mortality were modeled as function of each individual GI symptom (i.e., nausea, vomiting and diarrhea) and any GI symptoms, and covariates including age, gender, BMI, hypertension, diabetes, lung and heart diseases. This plot shows the sign of association of each GI symptom and the covariates which were found significant across different GI symptoms models. **d,** Confidence intervals of odds ratio (95%) of GI symptoms based on 1000 bootstrap iterations based on multivariate logistic regression for severity (blue) and mortality (red). **e,** Validation based on the external cohort. Confidence intervals of odds ratio (95%) of diarrhea covariate based on 1000 bootstrap iterations to capture mortality, ICU and composite outcome of ICU admission or death. Results are based on multivariate models after accounting for confounders such as BMI, age, gender, lung disease, heart diseases and hypertension. **f,** Validation and prediction model based on the internal cohort. Boxplot of AUC over 1000 bootstrap iterations to predict Mortality and Severity status in the validation cohort (top panel). Confidence intervals of the reduction in AUC (95%) based on 1000 bootstrap iterations for the model “Age + BMI + Any GI Symptoms” after removing age (blue), GI symptoms (red) and BMI (dark-green).

Fig. 2: COVID-19 patients with GI symptoms have reduced levels of circulating inflammatory cytokines.

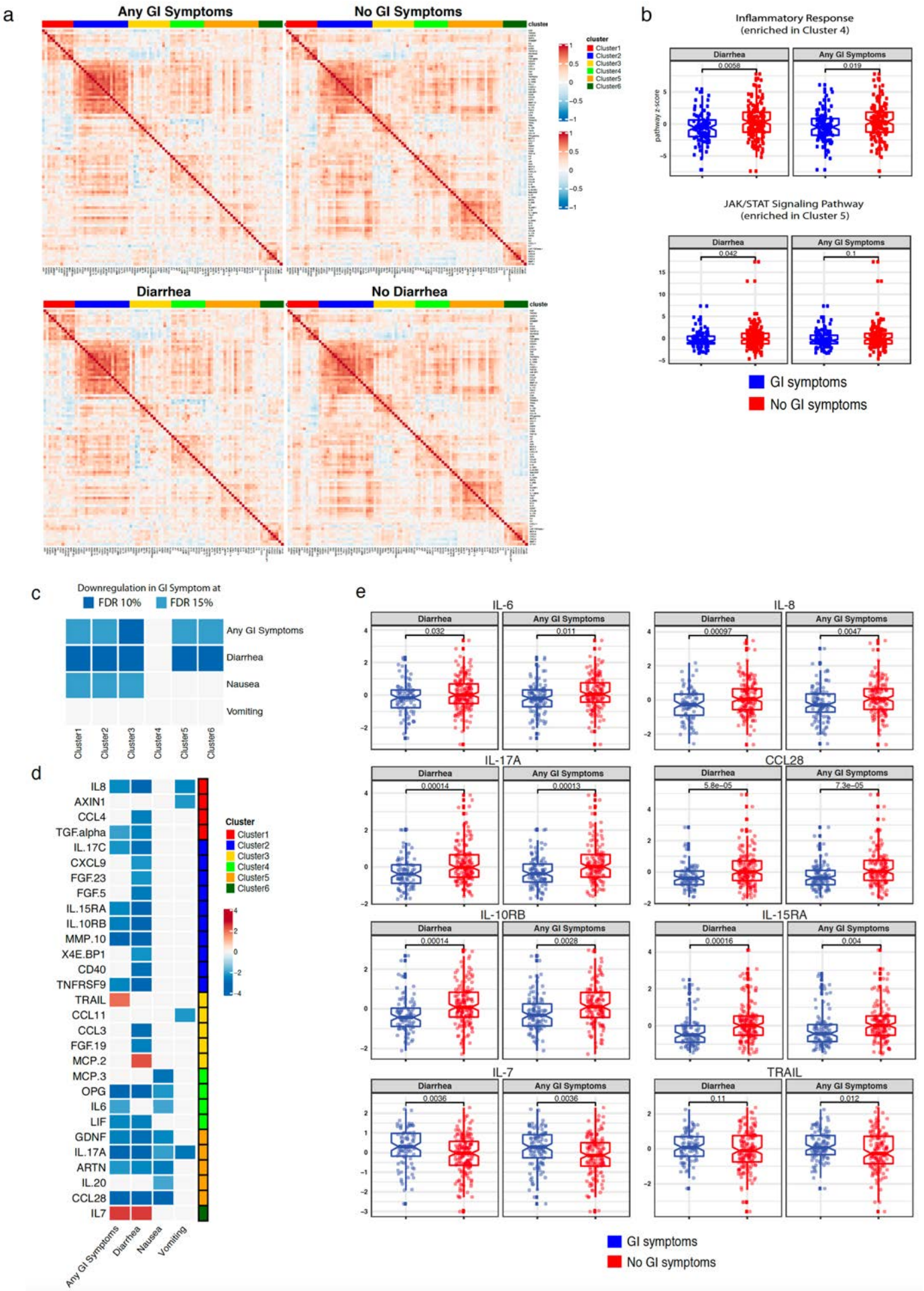

a, Correlation matrix (Pearson's) for 92 markers contained in multiplexed proteomic platform (Olink) across patients with any GI symptoms (top left panel) compared with no GI symptoms (top right panel) and patients with diarrhea (bottom left panel) compared with patients without diarrhea (bottom right panel). Cluster assignment derived based on consensus clustering is reported on the top of the heatmap. **b,** Boxplot of "Hallmark Inflammatory Response" and "KEGG JAK/STAT Signaling pathway" z-scores stratified by GI symptoms. P-values from unpaired t-tests are reported. "Hallmark Immune Response" and "Hallmark JAK/STAT Signaling" pathways were found significantly enriched at 10% FDR in Cluster 4 and Cluster 5, respectively. **c,** Association between proteomic clusters and GI symptoms. This association was derived by comparing clusters signatures between asymptomatic and symptomatic groups via t-test. Associations significant at 10% (dark blue) and 15% (light blue) FDR are reported. **d,** Analytes associated with GI symptoms at 10% FDR based on unpaired t-test. The intensity of the color is proportional to the -log10 p-value. Negative associations are displayed in blue; while positive associations in red. On the right side of the heatmap, the cluster assignment for each marker is reported. **c,** Boxplot of select differentially expressed markers stratified by GI symptoms. P-values from unpaired t-tests are reported.

Fig. 3: Clinical timing and histologic and endoscopic features of COVID-19 in the small intestine.

a.

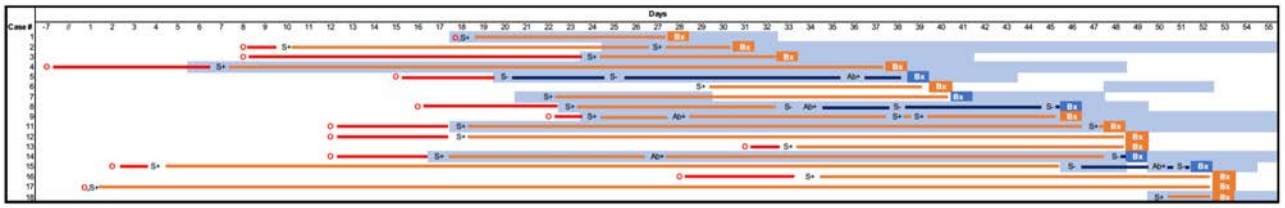

b.

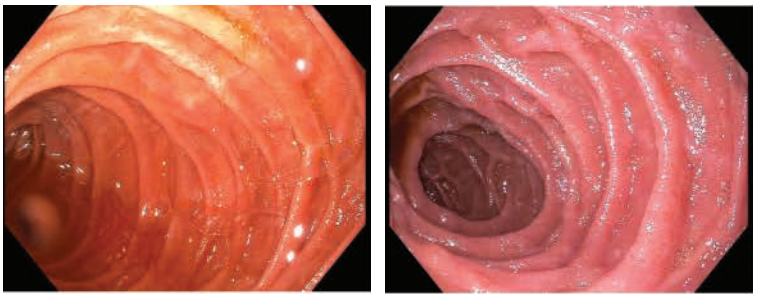

c.

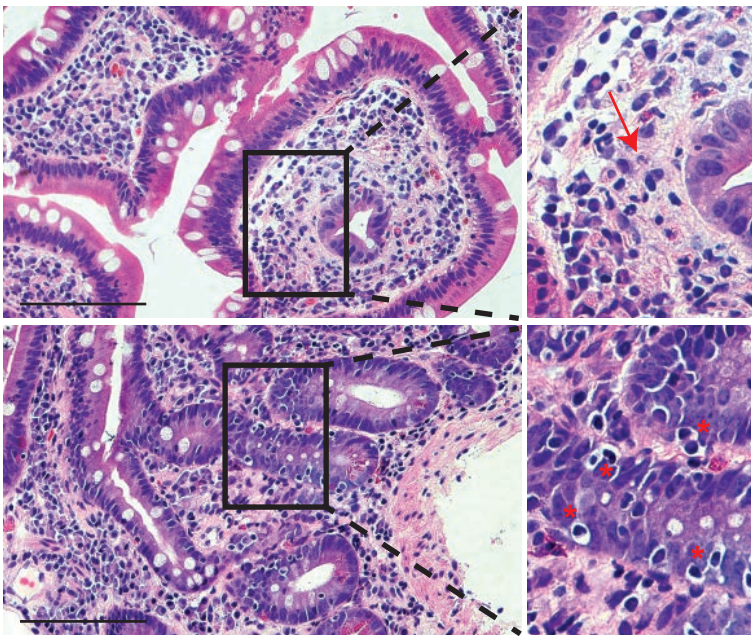

d.

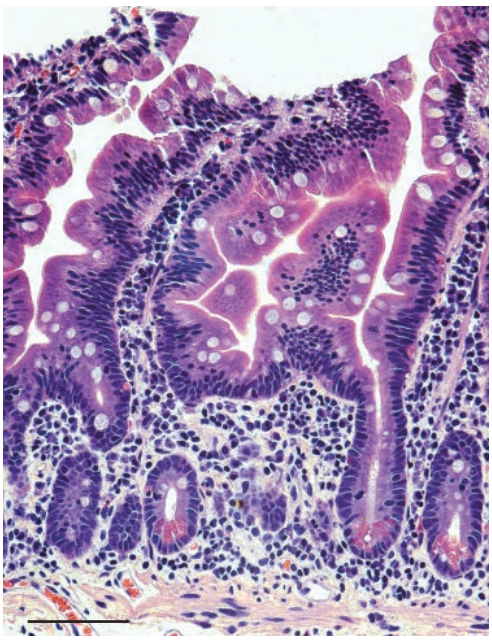

a, Timing of endoscopic evaluation with respect to COVID-19 course. **b,** Representative endoscopic views of the duodenum in COVID-19+ (left) and control (right) subjects. **c,** Histologic signs of inflammation detected in duodenal biopsies of COIVD-19 patients including neutrophils (arrow) and increased intraepithelial lymphocytes (*). **d,** Histologically normal duodenal tissue in a COVID-19 patient. Scale bar; 100 μm.

Fig. 4: SARS-CoV-2 viral particles and protein are detectable in intestinal tissue of COVID-19 patients.

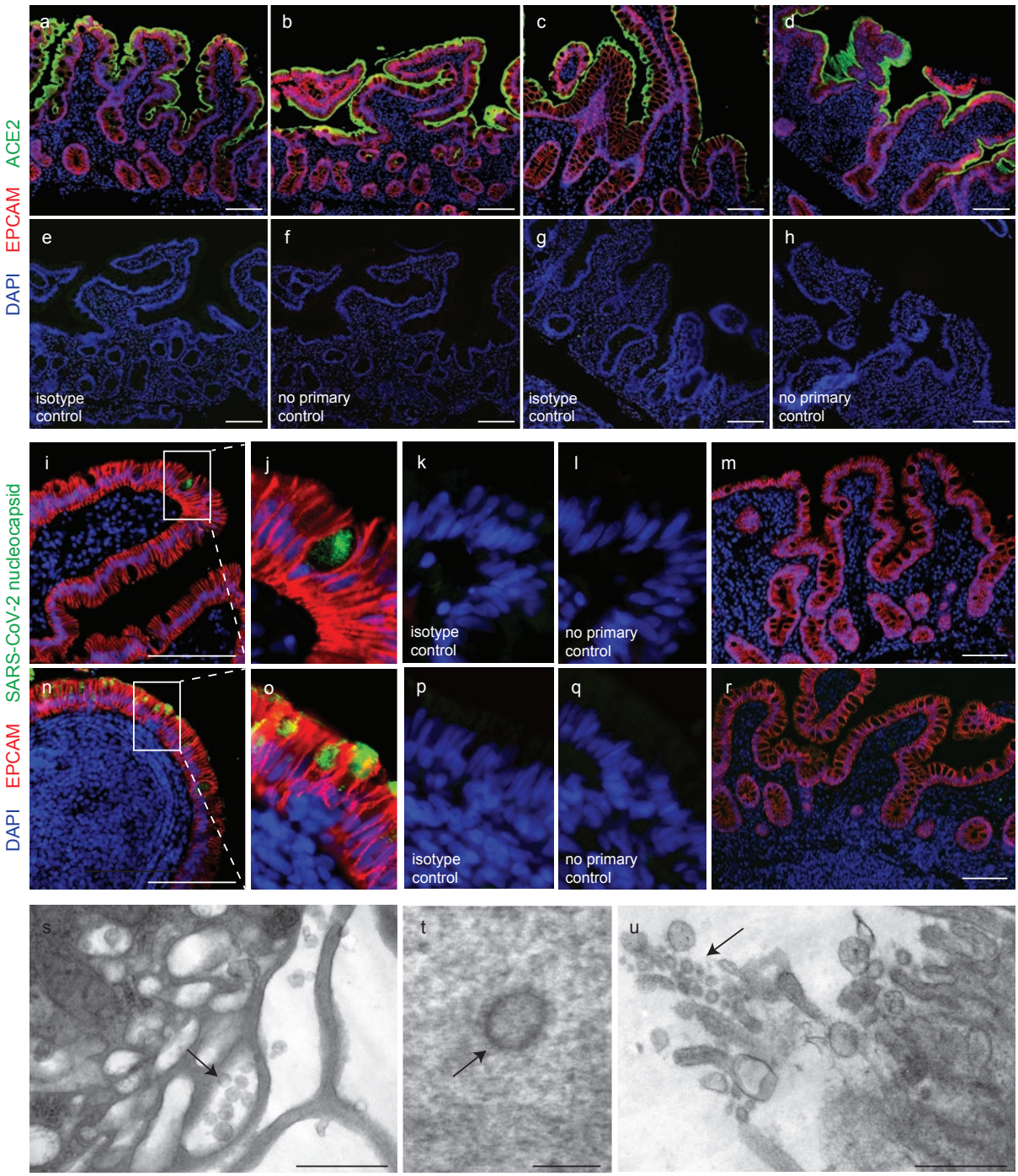

a-h, Immunofluorescent staining of duodenal **(a,b)** and ileal **(c,d)** biopsies of COVID-19 patients **(b,d)** and controls **(a,c)** with ACE2 (green), EPCAM(red) and DAPI (blue) including isotype **(e,g)** and no primary **(f,h)** controls.

i-r, Immunofluorescent staining of duodenal **(i-m)** and ileal **(n-q)** biopsies from COVID-19 patients **(i-l, n-q)** and controls **(m,r)** with SARS-CoV-2 nucleocapsid (green), EPCAM (red) and DAPI (blue) including isotype **(k,p)** and no primary **(j,q)** controls.

s-u, Electron microscopy of duodenal biopsies **(s, t)** and an ileal biopsy **(u)** from COVID-19 patients showing viral particles (arrows). Scale bars; 100 µm **(a-r)**, 0.5 µm **(s,u)**, 0.1 µm **(t)**.

Fig. 5: Identification of immune cell signatures in intestinal biopsies and blood from COVID-19 patients and controls based on mass cytometry.

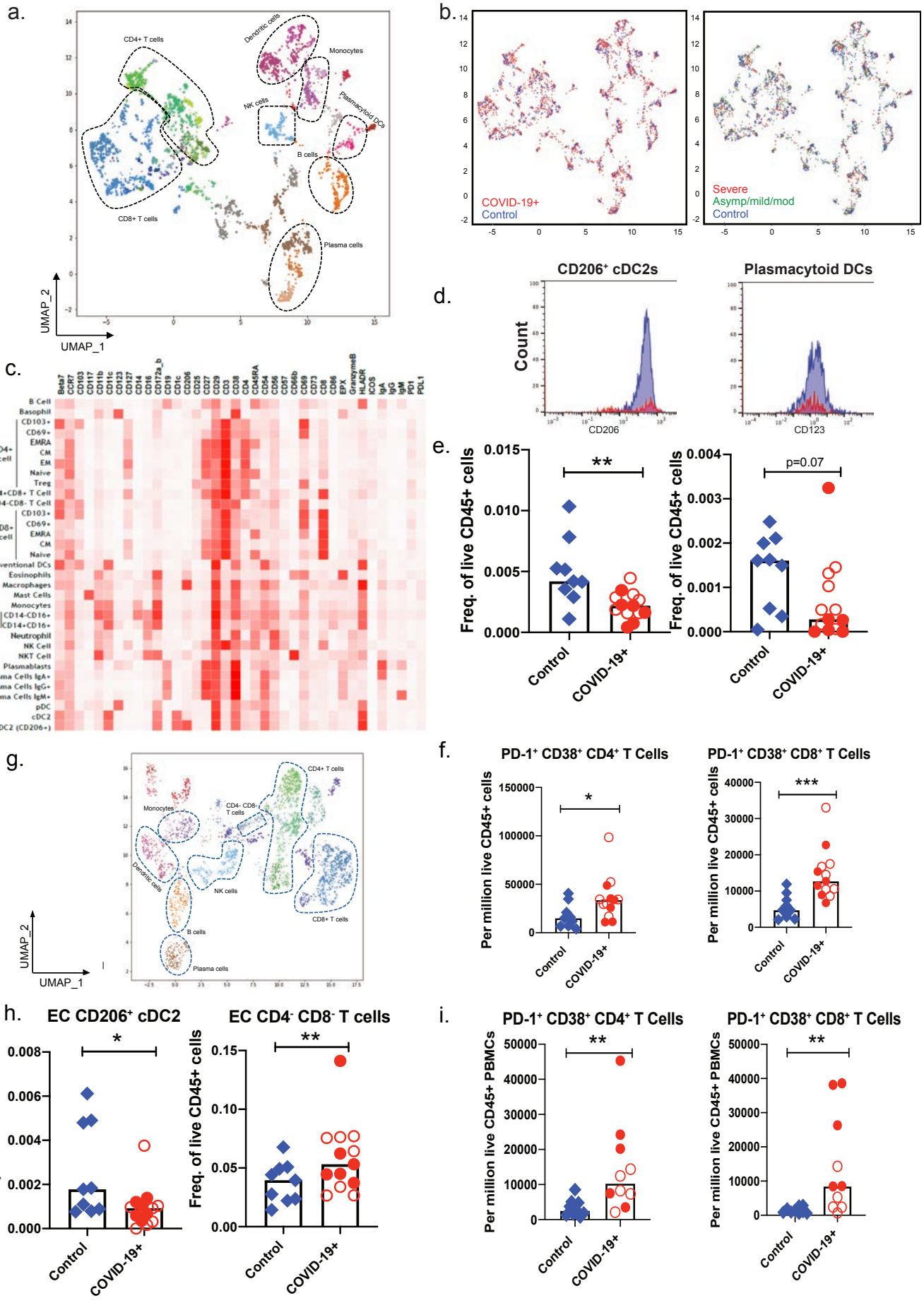

a, Uniform Manifold Approximation and Projection (UMAP) presentation of the eight clusters of immune populations based on 38 markers in lamina propria. **b,** UMAP presentation of clusters defined by COVID-19 (Red) vs Controls (Blue) and clusters defined by cohort where controls are indicated in blue, severe COVID-19 patients indicated in red and asymptomatic/mild/moderate COVID-19 patients are indicated in green in lamina propria. **c,**The heatmap shows the different immune populations based on specific cell type markers in lamina propria of COVID-19 patients and controls. **d,** The histograms shows the decrease in the expression of CD206 and CD123 in dendritic cell populations of COVID-19 patients (red) compared to the controls (blue). **e,** Unsupervised analyses of immune cells: The bar plots show the relative frequencies of different myeloid and lymphocytic immune populations namely CD206+ cDC2 and plasmacytoid DCs in lamina propria of controls (blue) and COVID-19 patients (red).. **f,** Supervised analyses: The bar graphs depict alterations in PD-1+ CD38+ (exhausted) CD4+ and CD8+ T cell subsets in lamina propria of controls (blue) and COVID-19 patients (red). **g,** Uniform manifold approximation and projection (UMAP) presentation of the eight clusters of immune populations based on 38 markers in epithelial compartment of small intestinal biopsies. **h,** Unsupervised analyses of immune cells: The bar plots show the relative frequencies of CD206+ cDC2 dendritic cells and CD4- CD8- T cells in the intraepithelial compartment of controls (blue) and COVID-19 patients (red). **i,** Supervised analyses on PBMCs indicating immune cell changes in blood : The bar graphs depict alterations in PD-1+ CD38+ (exhausted) CD4+ and CD8+ T cell subsets in blood of controls (blue) and COVID-19 patients (red).
Open red circles denote patients with asymptomatic/mild/moderate disease while filled red circles denote patients with severe COVID-19.

Fig. 6: Transcriptional changes in intestinal biopsies from COVID-19 patients against non-infected controls.

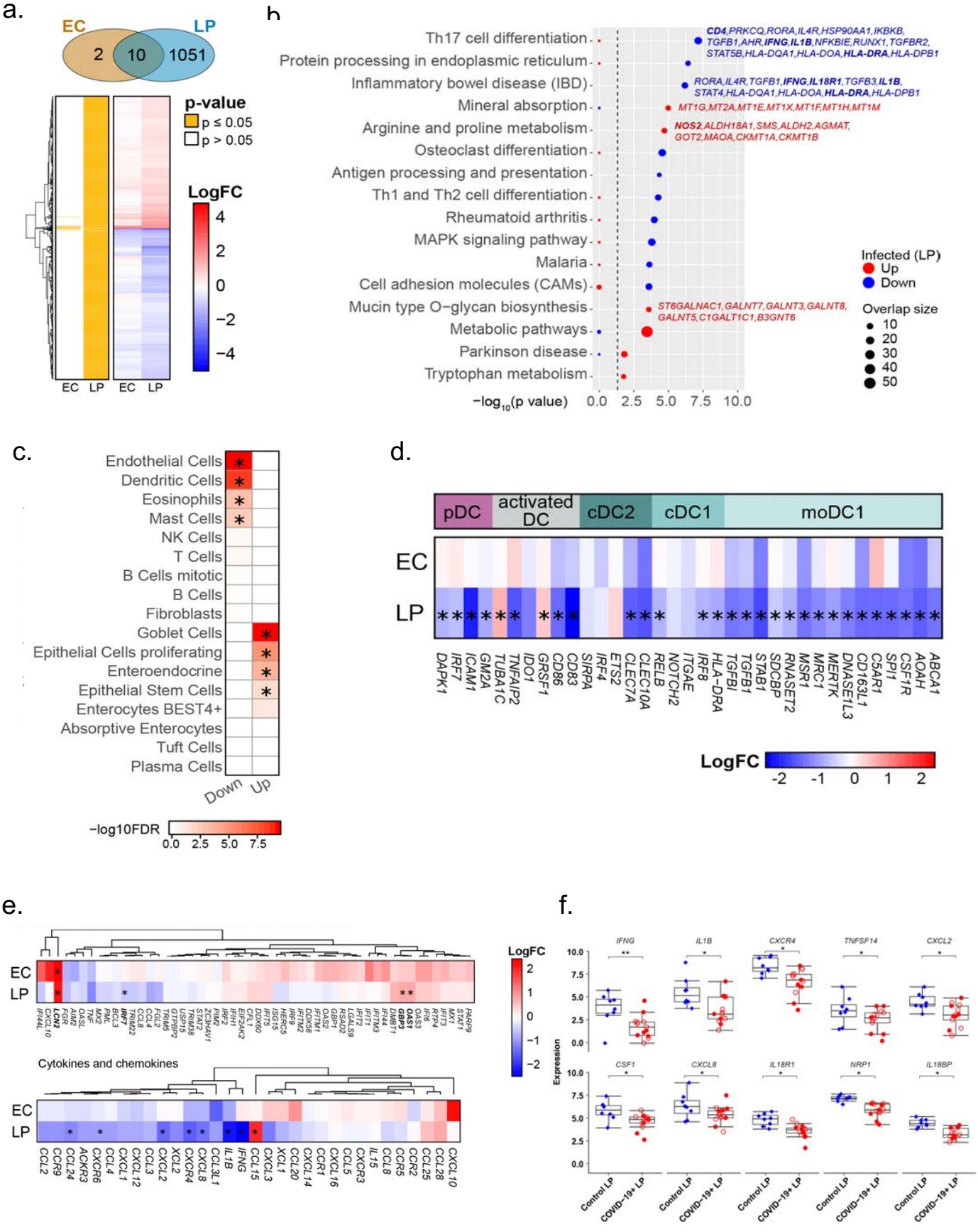

a, Hierarchical clustering of average expression changes for 1,063 genes (rows) with induced (red) or depleted (blue) expression (FDR ≤ 0.05) in the epithelial layer (EC) and lamina propria (LP) sections of intestinal biopsies from COVID-19 patients. The panel on the left indicates significant genes for each tissue section in yellow. The color bar indicates the average log2 fold-change (FC). **b,** Top enriched pathways (KEGG) induced (red) or depleted (blue) in LP. The dash line indicates the p ≤ 0.05 cutoff. Gene names for are indicated for main pathways related to inflammation and cell type composition. The dash line indicates the p ≤ 0.05 cutoff. **c,** Deconvolution of main intestinal (GI) cell types enriched or depleted in the LP section of COVID-19 convalescent patients against controls. Reference scRNA-seq cell type signatures were taken from Smillie et al 2019. (p ≤ 0.05, Fisher's exact test). **d,** Average expression changes for dendritic cell markers in the LP and EC sections. The yellow boxes indicate significant genes for each tissue section. The color bar indicates the average log2 fold-change (FC). **e,** Hierarchical clustering of average expression changes (columns) in the EC and LP sections for genes related to antiviral response to SARS-CoV-2 in post-mortem lung tissue of COVID-19 patients as described by Blanco-Mello et al. 2020 (top panel) and for cytokines and chemokines (bottom panel). Significant genes are indicated by the asterisks. The color bar indicates the average log2 fold-change (FC). **f,** The gene expression levels for the top 10 significant chemokines and cytokines in the LP section of COVID-19 patients (13) and controls (8). **p* < 0.05, ***p* < 0.01. Open red circles denote patients with asymptomatic/mild/moderate disease while filled red circles denote patients with severe COVID-19.